AFRL-RX-TY-TR-2008-4552

DEVELOPMENT OF A SINGLE DEGREE-OF-FREEDOM (SDOF) MODEL FOR AN ALUMINUM ARCH SUBJECTED TO IMPULSE LOADS

James S. Davidson and David P. Ray
University of Alabama at Birmingham
1075 13th Street South
Birmingham, AL 35294

Robert J. Dinan
Air Force Research Laboratory
139 Barnes Drive, Suite 2
Tyndall Air Force Base, FL 32403-5323

Contract No. FA4819-07-D-0001

July 2007

.

AIR FORCE RESEARCH LABORATORY
MATERIALS AND MANUFACTURING DIRECTORATE

■ **Air Force Materiel Command** ■ **United States Air Force** ■ **Tyndall Air Force Base, FL 32403-5323**

DISCLAIMER

Reference herein to any specific commercial product, process, or service by trade name, trademark, manufacturer, or otherwise does not constitute or imply its endorsement, recommendation, or approval by the United States Air Force. The views and opinions of authors expressed herein do not necessarily state or reflect those of the United States Air Force.

This report was prepared as an account of work sponsored by the United States Air Force. Neither the United States Air Force, nor any of its employees, makes any warranty, expressed or implied, or assumes any legal liability or responsibility for the accuracy, completeness, or usefulness of any information, apparatus, product, or process disclosed, or represents that its use would not infringe privately owned rights.

NOTICE AND SIGNATURE PAGE

Using Government drawings, specifications, or other data included in this document for any purpose other than Government procurement does not in any way obligate the U.S. Government. The fact that the Government formulated or supplied the drawings, specifications, or other data does not license the holder or any other person or corporation; or convey any rights or permission to manufacture, use, or sell any patented invention that may relate to them.

This report was cleared for public release by the 88th Air Base Wing Public Affairs Office at Wright Patterson Air Force Base, Ohio and is available to the general public, including foreign nationals. Copies may be obtained from the Defense Technical Information Center (DTIC) (http://www.dtic.mil).

AFRL-RX-TY-TR-2008-4552 HAS BEEN REVIEWED AND IS APPROVED FOR PUBLICATION IN ACCORDANCE WITH ASSIGNED DISTRIBUTION STATEMENT.

LOWERY.JASON.P.1292831621 Digitally signed by LOWERY.JASON.P.1292831621 DN: c=US, o=U.S. Government, ou=DoD, ou=PKI, ou=USAF, cn=LOWERY.JASON.P.1292831621 Date: 2012.03.16 14:24:11 -05'00'

JASON P. LOWERY, 2nd Lt, USAF

Work Unit Manager

KENSKY.EUGENE.T.1230563450 Digitally signed by KENSKY.EUGENE.T.1230563450 DN: c=US, o=U.S. Government, ou=DoD, ou=PKI, ou=USAF, cn=KENSKY.EUGENE.T.1230563450 Date: 2012.06.08 09:35:58 -05'00'

EUGENE T. KENSKY, DR-III

Airbase Engineering Development Branch

RHODES.ALBERT.N.III.1175488622 Digitally signed by RHODES.ALBERT.N.III.1175488622 DN: c=US, o=U.S. Government, ou=DoD, ou=PKI, ou=USAF, cn=RHODES.ALBERT.N.III.1175488622 Date: 2012.07.17 12:38:33 -05'00'

ALBERT N. RHODES, PhD

Chief, Airbase Technologies Division

This report is published in the interest of scientific and technical information exchange, and its publication does not constitute the Government's approval or disapproval of its ideas or findings.

REPORT DOCUMENTATION PAGE

Form Approved
OMB No. 0704-0188

PLEASE DO NOT RETURN YOUR FORM TO THE ABOVE ADDRESS.

1. REPORT DATE *(DD-MM-YYYY)*	2. REPORT TYPE	3. DATES COVERED *(From - To)*
31-JUL-2007	Interim Technical Report	03-SEP-2002 -- 30-JUN-2007

4. TITLE AND SUBTITLE

Development of a Single-Degree-of-Freedom (SDOF) Model for an Aluminum Arch Subjected to Impulse Loads

5a. CONTRACT NUMBER

F08637-02-C-7027

5b. GRANT NUMBER

5c. PROGRAM ELEMENT NUMBER

0602102F

6. AUTHOR(S)

^Davidson, James S.; ^Ray, David P.; *Dinan, Robert J.

5d. PROJECT NUMBER

4915

5e. TASK NUMBER

F2

5f. WORK UNIT NUMBER

4915F24B

7. PERFORMING ORGANIZATION NAME(S) AND ADDRESS(ES)

^University of Alabama at Birmingham
1075 13th Street South
Birmingham, AL 35294

8. PERFORMING ORGANIZATION REPORT NUMBER

9. SPONSORING/MONITORING AGENCY NAME(S) AND ADDRESS(ES)

*Air Force Research Laboratory
Materials and Manufacturing Directorate
139 Barnes Drive, Suite 2
Tyndall Air Force Base, FL 32403-5323

10. SPONSOR/MONITOR'S ACRONYM(S)

AFRL/RXQF

11. SPONSOR/MONITOR'S REPORT NUMBER(S)

AFRL-RX-TY-TR-2008-4552

12. DISTRIBUTION/AVAILABILITY STATEMENT

Distribution Statement A: Releasable to the public; distribution unlimited.

13. SUPPLEMENTARY NOTES

Ref Public Affairs Case # 88ABW-2012-4552, 27 July 2012. Document contains color images.

14. ABSTRACT

This document was prepared to report the results of analysis performed to develop a static resistance definition for an aluminum arch similar to that used in soft-walled shelter frames. The static resistance curve was developed using a NAsa STRuctural ANalysis (NASTRAN) Finite Element Model of a single bay of the shelter system. Pressure loads were input to the model as a distributed load over the surface of the structure facing the impulse load within a nonlinear static NASTRAN analysis. The displacement resulting from the analysis was then used to develop the static resistance function. The resulting resistance function was then used in a single-degree-of-freedom (SDOF) model to predict the displacement of the system when subjected to impulse loads. This displacement was then compared to empirical results obtained from full-scale testing. In addition to the test impulse conditions, additional cases that simulate various charge sizes and standoff distances were input into the SDOF model. These conditions were chosen to simulate points on the pressure-impulse diagram that showed minor damage to the structure and failure of the structure when using the pressure-impulse diagram developed for the shelter through the test program.

15. SUBJECT TERMS

single degree of freedom, SDOF

16. SECURITY CLASSIFICATION OF:			17. LIMITATION OF ABSTRACT	18. NUMBER OF PAGES	19a. NAME OF RESPONSIBLE PERSON
a. REPORT	b. ABSTRACT	c. THIS PAGE			Robert J. Dinan
U	U	U	UU	68	19b. TELEPHONE NUMBER *(Include area code)*

Reset

Standard Form 298 (Rev. 8/98)
Prescribed by ANSI Std. Z39.18

TABLE OF CONTENTS

LIST OF FIGURES iii
LIST OF TABLES v
1. SUMMARY 1
2. INTRODUCTION AND BACKGROUND 2
2.1. Shelter Description 2
2.2. Test Results 3
3. FINITE ELEMENT MODELING METHODOLOGY 6
3.1. Model Description 6
3.2. Model Verification 6
3.3. Model Static Analysis 8
3.4. NASTRAN Static Analysis Methods 8
3.5. LS-DYNA Impulse Analysis Methods 8
4. DEVELOPMENT OF STATIC NONLINEAR RESISTANCE FUNCTION 9
4.1. Load Distribution 9
4.2. Analysis Method 12
4.3. Analysis Results 13
4.3.1. 2400 lb Load Case Results 13
4.3.2. 4800 lb Load Case Results 16
4.3.3. 7200 lb Load Case Results 19
4.4. Analysis Parametric Study 22
4.4.1. 2400 lb Load Case Results, Simply Supported 22
4.5. Static Resistance Function 23
4.5.1. Elastic Static Resistance Function 24
4.5.2. Plastic Static Resistance Function 24
4.5.3. Static Resistance Function Development 25
5. LS-DYNA IMPULSE LOAD SIMULATION RESULTS 26
5.1. 81.1 psi-ms Results 27
5.2. 55.7 psi-ms Results 28
5.3. 30.5 psi-ms Results 30
5.4. 94.8 psi-ms Results 31
5.5. 76.4 psi-ms Results 32
5.6. 55.0 psi-ms Results 34
5.7. 32.2 psi-ms Results 35
5.8. 111.0 psi-ms Results 37
5.9. 24.7 psi-ms Results 38
5.10. 116.8 psi-ms Results 40
5.11. 33.1 psi-ms Results 41
6. SDOF MODEL VERIFICATION 44
6.1. SDOF Analytical Development 44
6.2. SDOF Model Term Definition and Calculation 46
6.2.1. Applied Force (*Ft*) 46
6.2.2. Adjusted Time 47
6.2.3. Load Mass Factor (K_{LM}) 47
6.2.4. System Mass (*Mt*) 47
7. ANALYSIS CHARTS 48

7.1. Graphical Comparison of LS-DYNA and SDOF Results....48
8. SUMMARY AND CONCLUSIONS....61
9. REFERENCES....62
LIST OF SYMBOLS, ABBREVIATIONS, AND ACRONYMS....63

LIST OF FIGURES

Page
Figure 1. Assembled Shelter 2
Figure 2. Shelter Interior View 3
Figure 3. Large Impulse 4
Figure 4. Medium Impulse 4
Figure 5. Small Impulse 5
Figure 6. FEM Isometric View 6
Figure 7. Mode 1 Fnz = 5.9Hz, Effective Mass Participation = 53% 7
Figure 8. Mode 2 Fnz = 6.7Hz, Effective Mass Participation = 47% 8
Figure 9. Example NASTRAN Model Load Distribution 11
Figure 10. NASTRAN Model Load Distribution Section View 12
Figure 11. Stress vs. Strain Diagram 13
Figure 12. 2400 lb Load Case Deflection vs. Load Step 14
Figure 13. 2400 lb Load Case Yield Point 15
Figure 14. 2400 lb Load Case Maximum Deflection 15
Figure 15. 2400 lb Load Case Maximum Deflection Section View 16
Figure 16. 4800 Load Case Deflection vs. Load Step 17
Figure 17. 4800 lb Load Case Yield Point 18
Figure 18. 4800 lb Load Case Maximum Deflection 18
Figure 19. 4800 lb Load Case Maximum Deflection Section View 19
Figure 20. 4800 lb Load Case Deflection vs. Load Step 20
Figure 21. 7200 lb Load Case Yield Point 21
Figure 22. 7200 lb Load Case Maximum Deflection 21
Figure 23. 7200 lb Load Case Maximum Deflection Section View 22
Figure 24. 2400 lb Load Case Deflection vs. Load Step 23
Figure 25. Static Resistance Function 25
Figure 26. Deflection Recovery Node 27
Figure 27. Purlin Translation for 81.1 psi-ms 27
Figure 28. Arch Deflected Shape for 81.1 psi-ms 28
Figure 29. Arch Stress Distribution for 81.1 psi-ms 28
Figure 30. Purlin Translation for 55.7 psi-ms 29
Figure 31. Arch Deflected Shape for 55.7 psi-ms 29
Figure 32. Arch Stress Distribution for 55.7 psi-ms 29
Figure 33. Purlin Translation for 30.5 psi-ms 30
Figure 34. Arch Deflected Shape for 30.5 psi-ms 30
Figure 35. Arch Stress Distribution for 30.5 psi-ms 31
Figure 36. Purlin Translation for 94.8 psi-ms 31
Figure 37. Arch Deflected Shape for 94.8 psi-ms 32
Figure 38. Arch Stress Distribution for 94.8 psi-ms 32
Figure 39. Purlin Translation for 76.4 psi-ms 33
Figure 40. Arch Deflected Shape for 76.4 psi-ms 33
Figure 41. Arch Stress Distribution for 76.4 psi-ms 34
Figure 42. Purlin Translation for 55.0 psi-ms 34
Figure 43. Arch Deflected Shape for 55.0 psi-ms 35
Figure 44. Arch Stress Distribution for 55.0 psi-ms 35

Figure 45. Purlin Translation for 32.2 psi-ms 36
Figure 46. Arch Deflected Shape for 32.2 psi-ms 36
Figure 47. Arch Stress Distribution for 32.2 psi-ms 37
Figure 48. Purlin Translation for 111.0 psi-ms 37
Figure 49. Arch Deflected Shape for 111.0 psi-ms 38
Figure 50. Arch Stress Distribution for 111.0 psi-ms 38
Figure 51. Purlin Translation for 24.7 psi-ms 39
Figure 52. Arch Deflected Shape for 24.7 psi-ms 39
Figure 53. Arch Stress Distribution for 24.7 psi-ms 40
Figure 54. Purlin Translation for 116.8 psi-ms 40
Figure 55. Arch Deflected Shape for 116.8 psi-ms 41
Figure 56. Arch Stress Distribution for 116.8 psi-ms 41
Figure 57. Purlin Translation for 33.1 psi-ms 42
Figure 58. Arch Deflected Shape for 33.1 psi-ms 42
Figure 59. Arch Stress Distribution for 33.1 psi-ms 43
Figure 60. Load Distribution—81.1 psi-ms 49
Figure 61. Displacement with Reflected Impulse of 81.1 psi-ms 49
Figure 62. SDOF/LS/DYNA Model Displacement Comparison—81.1 psi-ms 50
Figure 63. Load Distribution—55.7 psi-ms 50
Figure 64. Displacement with Reflected Impulse of 55.7 psi-ms 50
Figure 65. SDOF/LS-DYNA Model Displacement Comparison—55.7 psi-ms 51
Figure 66. Load Distribution—30.5 psi-ms 51
Figure 67. Displacement with Reflected Impulse of 30.5 psi-ms 52
Figure 68. SDOF/LS-DYNA Model Displacement Comparison—30.5 psi-ms 52
Figure 69. Load Distribution—94.8 psi-ms 52
Figure 70. Displacement with Reflected Impulse of 94.8 psi-ms 53
Figure 71. SDOF/LS-DYNA Model Displacement Comparison—94.8 psi-ms 53
Figure 72. Load Distribution—76.4 psi-ms 53
Figure 73. Displacement with Reflected Impulse of 76.4 psi-ms 54
Figure 74. SDOF/LS-DYNA Model Displacement Comparison—76.4 psi-ms 54
Figure 75. Load Distribution—55.0 psi-ms 54
Figure 76. Displacement with Reflected Impulse of 55.0 psi-ms 55
Figure 77. SDOF/LS-DYNA Model Displacement Comparison—55.0 psi-ms 55
Figure 78. Load Distribution—32.2 psi-ms 55
Figure 79. Displacement with Reflected Impulse of 32.2 psi-ms 56
Figure 80. SDOF/LS-DYNA Model Displacement Comparison—32.2 psi-ms 56
Figure 81. Load Distribution—111.0 psi-ms 56
Figure 82. Displacement with Reflected Impulse of 111.0 psi-ms 57
Figure 83. SDOF/LS-DYNA Model Displacement Comparison—111.0 psi-ms 57
Figure 84. Load Distribution—24.7 psi-ms 57
Figure 85. Displacement with Reflected Impulse of 24.7 psi-ms 58
Figure 86. SDOF/LS-DYNA Model Displacement Comparison—24.7 psi-ms 58
Figure 87. Load Distribution—116.8 psi-ms 58
Figure 88. Displacement with Reflected Impulse of 116.8 psi-ms 59
Figure 89. SDOF/LS-DYNA Model Displacement Comparison—116.8 psi-ms 59
Figure 90. Load Distribution—33.1 psi-ms 59

Figure 91. Displacement with Reflected Impulse of 33.1 psi-ms 60
Figure 92. SDOF/LS-DYNA Model Displacement Comparison—33.1 psi-ms 60

LIST OF TABLES

Page

Table 1. Test Loads 3
Table 2. Damage Level 3
Table 3. Load Calculation for NASTRAN 2400 lb Nonlinear Load Application, P_{max} 100 lbs .. 10
Table 4. Load Calculation for NASTRAN 4800 lb Nonlinear Load Application, P_{max} 200 lbs .. 10
Table 5. Load Calculation for NASTRAN 7200 lb Nonlinear Load Application, P_{max} 300 lbs .. 11
Table 6. 2400 lb Load Case Deflection 14
Table 7. 4800 lb Load Case Deflection 16
Table 8. 7200 lb Load Case Deflection 20
Table 9. 2400 lb Load Case Deflection, Simply Supported Base 23
Table 10. Elastic Stiffness Summary 24
Table 11. Initial Plastic Stiffness Summary 24
Table 12. Second Plastic Stiffness Summary 25
Table 13. Model Impulse Analysis Results 26
Table 14. SDOF Parameters 48
Table 15. LS-DYNA/SDOF Results Comparison 48
Table 16. Initial Conditions 49

1. SUMMARY

Quick and accurate prediction of damage to structures from impulse loading resulting from blasts could provide a useful tool in situations where deployment of nonpermanent structures for housing of personnel and equipment is required. The ability to predict the required protected area for shelters in relation to the potential threat of blast loads would provide planners and personnel a valuable tool for use in the protection of life and property. Prediction curves can be developed through the testing of each type of structure using multiple charge sizes and standoff distances. However, this approach is inefficient in that is must be performed for each type of desired structure and in addition, only provides a few data points, which must then be extrapolated to encompass the myriad of potential combinations of charge size and standoff distance. A better tool would be an analytical model that is quick and simple to use, can be modified for multiple shelter types and, most importantly, is accurate across multiple shelter types.

This document was prepared to report the results of analysis performed to develop a static resistance definition for an aluminum arch similar to that used in soft walled shelter frames. The static resistance curve was developed using a NASA Structural Analysis Program (NASTRAN) finite element model (FEM) of a single bay of the shelter system. Pressure loads were input to the model as a distributed load over the surface of the structure facing the impulse load within a nonlinear static NASTRAN analysis. The displacement resulting from the analysis was then used to develop the static resistance function. The resulting resistance function was then used in a single-degree-of-freedom (SDOF) model to predict the displacement of the system when subjected to impulse iv loads. This displacement was then compared to empirical results obtained from full-scale testing. In addition to the test impulse conditions, additional cases that simulate various charge sizes and standoff distances were input into the SDOF model. These conditions were chosen to simulate points on the pressure-impulse diagram that showed minor damage to the structure and failure of the structure when using the pressure-impulse diagram developed for the shelter through the test program.

Additional analyses of the frame were then performed using LS-DYNA finite element software to predict damage from impulse loading. The same load cases used within the test program and the SDOF model were simulated within LS-DYNA. In addition to reporting the results of the static resistance curve for the arch frame, this document serves to document the correlation between test results, SDOF analysis results, and LS-DYNA analysis results.

2. INTRODUCTION AND BACKGROUND

A variety of temporary shelters comprised of circular metal arch frames are commercially available and are being used for many purposes. When used for military operations, these shelters may be exposed to external attacks by terrorists or others intent on inflicting harm to personnel and equipment located within the shelter. Full-scale tests have been used to understand the response of shelters to external blast loads. However, conducting full-scale explosive tests of these structures is a costly and time-consuming task. Therefore, it would be advantageous to have proven techniques to simulate impulse loading of the shelters without having to perform full-scale tests and also, the ability to correlate analysis results with test results.

2.1. Shelter Description

A typical metal arch frame shelter, the Alaska Small Shelter System (AKSSS), is shown in Figure 1. It consists of an aluminum frame covered by a vinyl fabric that is attached to an aluminum base. The structure is formed by attaching five arched bays to the aluminum base. These bays are connected by purlins that span the length of the shelter and attach to each bay. In addition, each bay is attached to the aluminum base on either side of the shelter. The ends of the shelter are enclosed by additional vinyl fabric that provides a reinforced entry way and windows. The sides of the shelter contain flaps that may be opened to provide ventilation to the structure. Figure 2 provides an interior view of the subject article.

Figure 1. Assembled Shelter

Figure 2. Shelter Interior View

2.2. Test Results

Full-scale explosive tests have been conducted on various shelters including the AKSSS. One test series was conducted in a joint operation between the United States Army Engineer Research and Development Center (ERDC) and the Air Force Research Laboratory (AFRL). This test, named Joint Soldier Protection in Contingency Environments (SPICE), provided test data for shelters exposed to three charge sizes, with multiple shelters used for each charge size. Table 1 provides a summary of the impulse loads involved in these tests, and Table 2 provides damage level definitions based on displacement measured at the purlins.

Table 1. Test Loads

Test	Reflected Impulse (psi-ms)
1B	81.1
1B	55.7
1B	30.5
2	94.8
2	76.4
2	55.0
2	32.2
3	251.0
3	206.4
3	175.3
3	152.2
3	109.0
3	109.0

Table 2. Damage Level

Level	Damage Level (in)
Minor	Greater than 4 but less than 14
Severe	Greater than 14 but less than 20
Failure	Greater than 20

Figure 3–Figure 5 were taken post test and provide a visual reference to the damage each shelter received in relation to its proximity to the charge. Also included in the test report is a graph of the conventional weapons effect (CONWEP) predicted reflected pressure versus CONWEP predicted reflected impulse with damage predictions overlaid on the graph. This graph presents the test results in a user-friendly format that allows the end user to quickly assess potential shelter damage from anticipated impulse load conditions.

Figure 3. Large Impulse

Figure 4. Medium Impulse

Figure 5. Small Impulse

It should be noted that the predicted reflected impulse was reduced by 45% to 70% due to the flexibility of the shelter not presenting an ideal reflecting surface. The test report provides additional insight into this reduction and the test methods behind the reduction rationale.

3. FINITE ELEMENT MODELING METHODOLOGY

The frame was modeled using FEMAP as the preprocessor for model generation, model constraint, and model loading. To simplify the model, only one bay of the frame was included in the FEM. Figure 6 provides an isometric view of the single bay FEM.

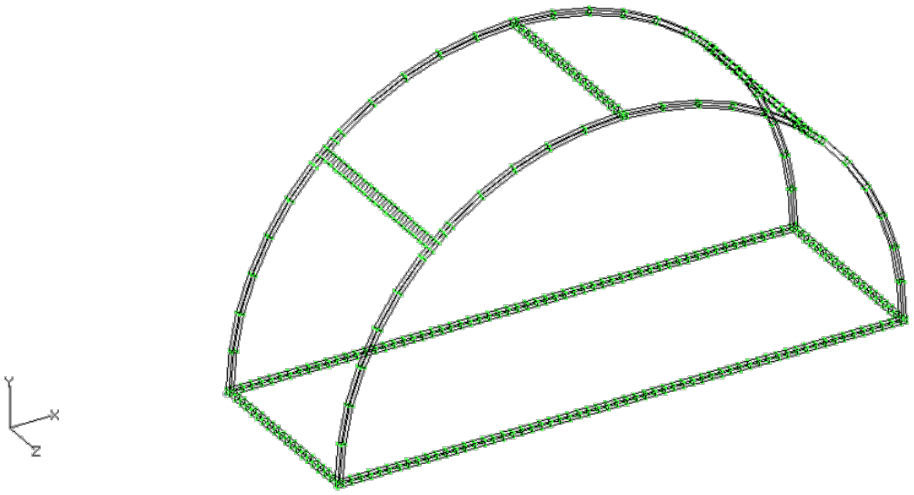

Figure 6. FEM Isometric View

3.1. Model Description

The frame was modeled using 1132 plate elements to form a four-sided hollow beam element. Each plate element is 2 in wide by 0.1 in thick. The plate elements were chosen for the model in anticipation of their use with the LS-DYNA solver which requires plate elements for use with the blast loading card. Figure 6 provides a view of the single bay with the purlins included along the length. The coordinate system for the model was arbitrarily chosen to have the *x* axis across the arch Model Origin Purlins 8 with the *z* axis along the depth of the arch, the *y* axis out the top of the arch, and the origin as shown in Figure 6. The FEM includes the weight of the aluminum frame. The mass of the fabric covering the frame was neglected in the model. This assumption was made to simplify the modeling effort so that the attempt to correlate FEM with SDOF modeling could continue in order to determine the feasibility of using a simple SDOF to represent a flexible soft-walled structure. The base restraint was modeled by placing elements on the ground surface and restraining them in all six degrees of freedom. The frame was then attached to these restrained elements. A parametric study was performed for the base restraint to compare the impact of varying restraint conditions on analysis results. This analysis is presented in Section 4.4.

3.2. Model Verification

Before proceeding with the static analysis, the FEM was verified for completeness and accuracy by a series of model verification steps. The first method was to run a rigid-body mode check of the model. The FEMAP model was exported into a NASTRAN data deck, and all external constraints were removed from the model. Once the data deck was appropriately configured for a

real eigenvalue analysis, the Nx NASTRAN solver was used to extract the first 10 natural frequencies from the model. Even though only six rigid body modes were expected, 10 natural frequencies were requested to verify that no additional rigid body modes existed. As expected, the analysis returned six zero frequencies. The second verification method was to run a normal mode analysis, once again using Nx NASTRAN, and analyze the mode shapes against the mode shapes intuitively expected from the model. The two predominate 9 modes returned from the normal modes analysis is shown in Figure 7 and Figure 8. These figures also include the mode direction and effective mass participation in the mode as a percentage of total mass as calculated by the NASTRAN model. The final verification was to check the mesh fidelity to ensure that an adequate number of elements were used to accurately represent the behavior of the system. The model fidelity check was performed by constructing a simple beam element model and performing the same analyses that were requested for the shell element model. The results from the beam element model were checked against the results previously obtained from the shell element model and were found to be compatible. Therefore, due to the results from these three verification methods, the model was verified to be correct and of sufficient fidelity to provide accurate results.

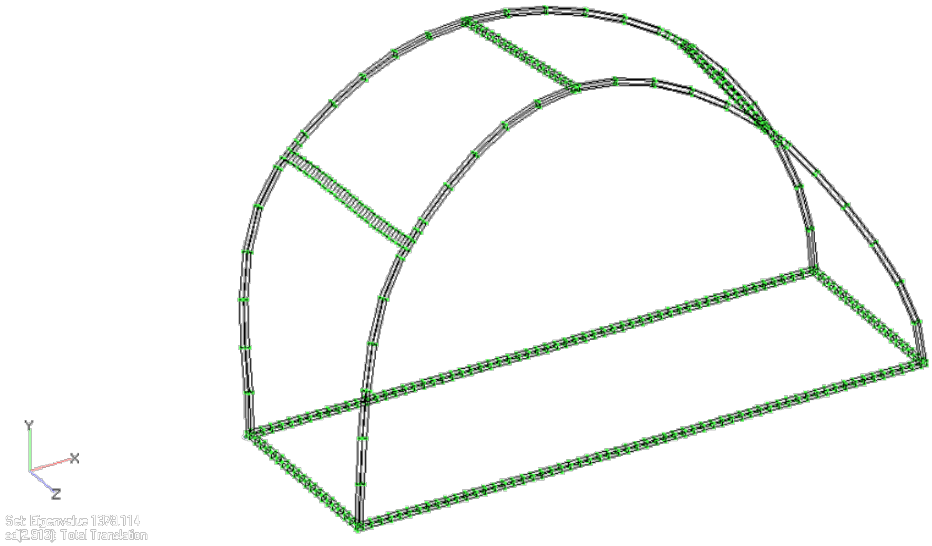

Figure 7. Mode 1 Fnz = 5.9Hz, Effective Mass Participation = 53%

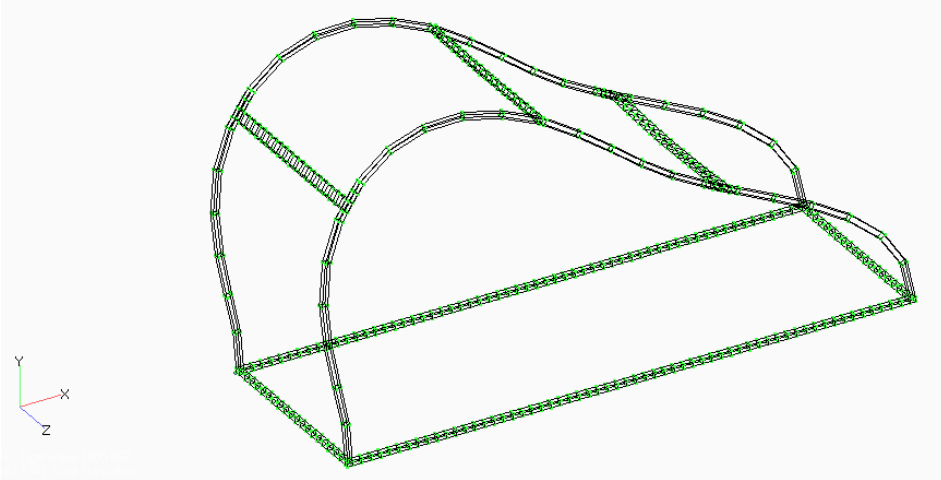

Figure 8. Mode 2 Fnz = 6.7Hz, Effective Mass Participation = 47%

3.3. Model Static Analysis

Test results were obtained by placing the test charge in a position that was normal to the long side of the structure. Therefore, to correlate the test results with the FEM results, all analyses were performed with the load applied parallel to the *x* axis in the positive *x* direction. Static analysis consisted of two distinct analyses. The first method was to apply a static load across the face of the shell elements and use NASTRAN to solve for the stresses within the frame. The second method was to export the FEMAP model to LS-DYNA and use the blast load card to simulate the test conditions reported in the test report.

3.4. NASTRAN Static Analysis Methods

Initial NASTRAN runs were made using unit loads applied across the surface of the frame. These solutions, along with additional NASTRAN linear and nonlinear static 11 solutions will be required to develop the SDOF model for the frame. Additional detail of this analysis is contained in Section 5.

3.5. LS-DYNA Impulse Analysis Methods

The FEM was exported into a LS-DYNA format directly from FEMAP. A LOAD_BLAST card was inserted into the LS-DYNA data deck to represent different impulse loading conditions. Multiple impulse loads were analyzed through the model with special attention to impulse loads from the test report. Additional detail of this analysis is contained in Section 5

4. DEVELOPMENT OF STATIC NONLINEAR RESISTANCE FUNCTION

In order to develop a SDOF model, it is necessary to understand the deflection behavior of the system. When subjected to an impulse load in the *x* direction, the arch will have two distinct deflection phases, as it deflects in the elastic mode initially and then transitions to the plastic phase. The development of the static resistance function used the NASTRAN model of the system to perform a geometric and material static nonlinear analysis and establish the static resistance function of the system. Three separate analyses were performed using different load values. The three load values considered were 2400 lbs, 4800 lbs, and 7200 lbs, distributed over the two arches making up the structure. These load values were chosen such that the low end of the load only slightly exceeded the material yield point, while the high end greatly exceeded the material yield point and approached the deflection that was considered severe damage during the test program. The results of these three analyses were compared for consistency of results, especially for the elastic portion of the system. This analysis yielded a stiffness value for both the linear and nonlinear portions of the deflection of the system. The load distribution, analysis methods, and results for this analysis are described in the following sections.

4.1. Load Distribution

The static resistance function development used a load distribution equation to calculate the load that should be applied at multiple discreet points along the frame. This equation recognized that the frame will experience the highest loads on surfaces that are perpendicular to the impulse (base of frame), with the load decreasing to zero on surfaces 13 that are parallel to the load (top of frame). Therefore, the load used in the NASTRAN analysis was calculated for each point according to the following equation.

$$P = \left\lfloor \frac{P_{max}}{\frac{\pi}{2} * x} \right\rfloor * \left\lfloor \pi * \left(\frac{x}{2}\right) - x\left(\pi + \tan^{-1}\frac{y}{x}\right) \right\rfloor \quad (1)$$

P_{max} = maximum load point
$x = x$ coordinate of load point
$y = y$ coordinate of load point

Equation 1 provides an accurate load distribution as long as all points along the curve are equally distributed. If the points are not equally distributed, the load will be higher at the points that are closer together and lower at the points that are spaced farther apart. This load anomaly would occur in the model because the area near the purlin consists of a finer mesh because this is the area where deflection data is desired. The purlin area is broken into five discreet areas that are equivalent to the other eleven areas on each arch. To accommodate this finer mesh and keep the load distribution consistent, the load in the purlin area was averaged and applied over the five nodes in the area. Tables 3, 4, and 5 below provide the load distribution used in the static nonlinear analyses as calculated per Equation 1. The averaging of the load at points 6-10 can be seen in the column titled “Final Load Distribution.” Also note that the difference between the column titled “P” and the column titled “Final Load Distribution” is not important as long as the load is distributed along the arch according to Equation 1, because the final total is used in the static resistance calculation, i.e. *K* = final load distribution/deflection. The load distributions shown in Tables 3, 4, and 5 were applied to each side of the two arch segments in the model to arrive at the final total load applied to the arch.

Table 3. Load Calculation for NASTRAN 2400 lb Nonlinear Load Application, P_{max} 100 lbs

Point	X (in)	Y (in)	P (lbs)	Theta (rad)	Final Load Distribution (lbs)
1	0.0	121.0	-0.1	0.00	0.0
2	-16.1	117.8	8.6	0.10	8.6
3	-31.1	116.8	16.5	0.21	16.5
4	-46.2	111.7	24.9	0.31	24.9
5	-61.1	104.5	33.7	0.42	33.7
6	-74.1	95.6	42.0	0.52	9.2
7	-77.1	93.3	43.9	0.63	9.2
8	-80.8	90.1	465	0.73	9.2
9	-82.2	88.8	47.5	0.84	9.2
10	-85.9	85.2	50.2	0.94	9.2
11	-97.3	71.3	59.7	1.05	59.7
12	-103.2	63.1	65.0	1.15	65.0
13	-112.9	44.1	76.3	1.26	76.3
14	-118.0	29.0	84.7	1.36	84.7
15	-119.9	14.4	92.4	1.47	92.4
16	-121.0	0.0	100	1.57	100.0
Sum			**791.9**		**607.8**

Table 4. Load Calculation for NASTRAN 4800 lb Nonlinear Load Application, P_{max} 200 lbs

Point	X (in)	Y (in)	P (lbs)	Theta (rad)	Final Load Distribution (lbs)
1	0.0	121.0	-0.1	0.00	0.0
2	-16.1	117.8	17.2	0.10	17.2
3	-31.1	116.8	33.0	0.21	33.0
4	-46.2	111.7	49.9	0.31	50.0
5	-61.1	104.5	67.3	0.42	67.4
6	-74.1	95.6	83.9	0.52	18.4
7	-77.1	93.3	87.9	0.63	18.4
8	-80.8	90.1	93.0	0.73	18.4
9	-82.2	88.8	95.1	0.84	18.4
10	-85.9	85.2	100.5	0.94	18.4
11	-97.3	71.3	119.4	1.05	119.4
12	-103.2	63.1	130.1	1.15	130.0
13	-112.9	44.1	152.6	1.26	152.6
14	-118.0	29.0	169.3	1.36	169.4
15	-119.9	14.4	184.8	1.47	184.8
16	-121.0	0.0	200.0	1.57	200.0
Sum			**1584**		**1215.8**

Table 5. Load Calculation for NASTRAN 7200 lb Nonlinear Load Application, P_{max} 300 lbs

Point	X (in)	Y (in)	P (lbs)	Theta (rad)	Final Load Distribution (lbs)
1	0.0	121.0	-0.2	0.00	0.0
2	-16.1	117.8	25.7	0.10	25.8
3	-31.1	116.8	49.5	0.21	49.5
4	-46.2	111.7	74.8	0.31	74.8
5	-61.1	104.5	101.0	0.42	101.0
6	-74.1	95.6	125.9	0.52	27.6
7	-77.1	93.3	131.8	0.63	27.6
8	-80.8	90.1	139.5	0.73	27.6
9	-82.2	88.8	142.6	0.84	27.6
10	-85.9	85.2	150.7	0.94	27.6
11	-97.3	71.3	179.1	1.05	179.1
12	-103.2	63.1	195.1	1.15	195.1
13	-112.9	44.1	228.8	1.26	228.8
14	-118.0	29.0	254.0	1.36	254.0
15	-119.9	14.4	277.2	1.47	277.2
16	-121.0	0.0	300.0	1.57	300.0
Sum			**2375.6**		**1823.3**

The load distribution and direction used in the NASTRAN model is further illustrated in Figure 9 and Figure 10 which are taken from the analysis model with the load distribution view turned on. As shown in these figures and discussed previously, the load is applied to nodes comprising each side of the two arches that are used in the model.

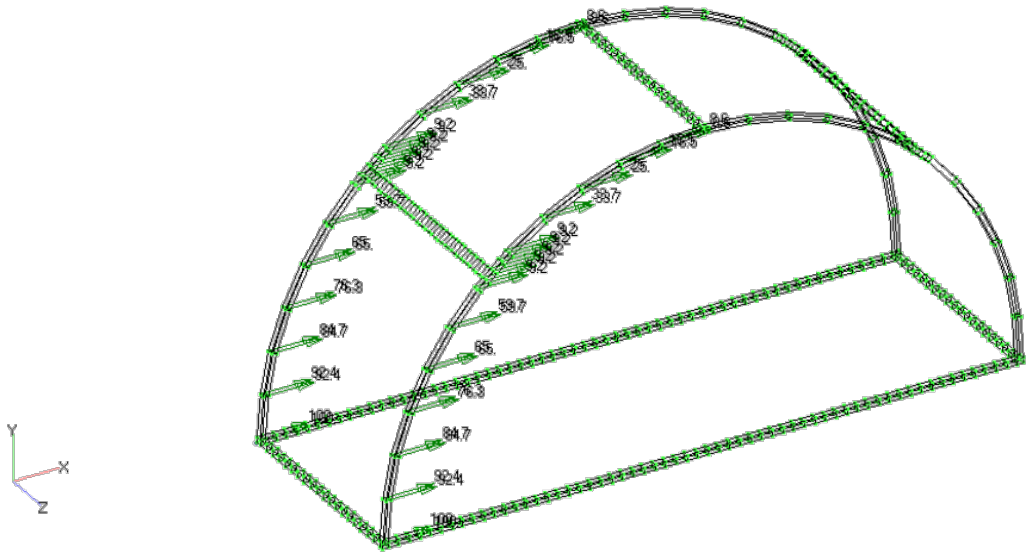

Figure 9. Example NASTRAN Model Load Distribution

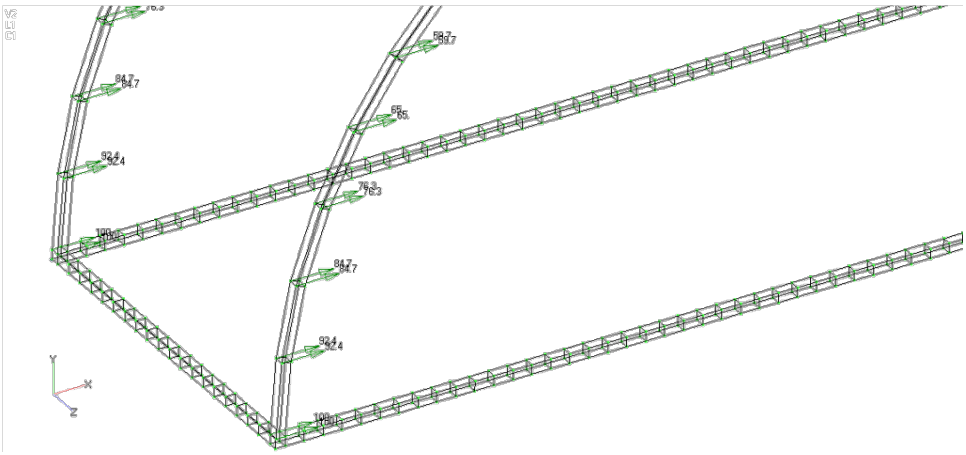

Figure 10. NASTRAN Model Load Distribution Section View

4.2. Analysis Method

The development of the resistance definition was accomplished using the static nonlinear solution method available in Nx NASTRAN. The load distribution described in Section 4.1 was applied to the model in 16 equally distributed load steps. Both geometric and material nonlinear analysis was conducted for each load distribution. For the material nonlinear analysis, the stress vs. strain diagram taken from the FEMAP preprocessor and shown in Figure 11 was used in the model. This function was used to represent the behavior of the material through and beyond the yield point. The stress strain diagram for Aluminum Alloy 6061-T6 as taken from MIL-HDBK-5H was used to represent the material of the frame. The material yield point is 35000 psi, with a material ultimate strength of 42000 psi (Figure 11). Geometric nonlinear behavior was modeled by using the PARAM LGDISP command in the NASTRAN Model. This allowed for the inclusion of follower forces and stiffness matrix updates, as the deflection in the model changed with increasing load. All three load distribution cases were run with large displacement effects turned both on and off in order to compare the results, which are discussed in Section 4.3. Deflections discussed in the following paragraph were taken from nodes located near the purlin interface with each arch. These nodes were chosen for their proximity to deflection sensors used in the test program on the actual structure.

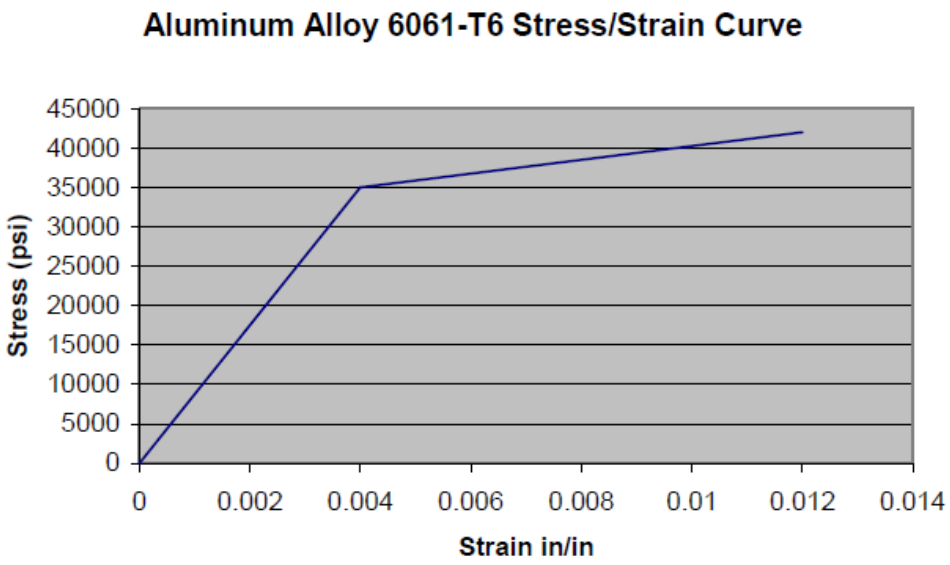

Figure 11. Stress vs. Strain Diagram

4.3. Analysis Results

The results of the two analysis load conditions are presented in this section. Each analysis consisted of running a material nonlinear analysis, then a geometric and material nonlinear analysis, and comparing the results. These results were then used to calculate a static resistance function.

4.3.1. 2400 lb Load Case Results

Table 6 provides a summary of the maximum deflection at the selected nodes in the model for the 2400 lb load case. As shown in the figures, the difference in deflection due to the inclusion of large displacements is negligible when compared to the overall deflection of the system.

As shown previously, there is no difference in deflection until the material yield point is reached. Once the material yields, however, the deflection is greater for the analysis that includes large deflection effects. This difference is negligible as it is only an increase of 0.9%. Figure 12 provides a graph of the deflection versus load step overlaid for the analysis, with large displacements turned both on and off.

Table 6. 2400 lb Load Case Deflection

Load step	Node	No large displacements		Large displacements included	
		Displacement (in)	Stress (psi)	Displacement (in)	Stress (psi)
1	1097	0.29	4319	0.29	4324
2	1097	0.58	8638	0.58	8658
3	1097	0.87	12957	0.87	13001
4	1097	1.16	17276	1.16	17353
5	1097	1.45	21596	1.45	21714
6	1097	1.74	25915	1.75	26084
7	1097	2.03	30235	2.04	30462
8	1097	2.32	34554	2.32	34859
9	951	2.62	35920	2.64	35995
10	951	2.93	36931	2.95	37010
11	951	3.24	37947	3.26	38094
12	951	3.58	39740	3.61	39913
13	951	3.93	41584	3.97	41763
14	951	4.28	43453	4.32	43650
15	951	4.63	45340	4.68	45546

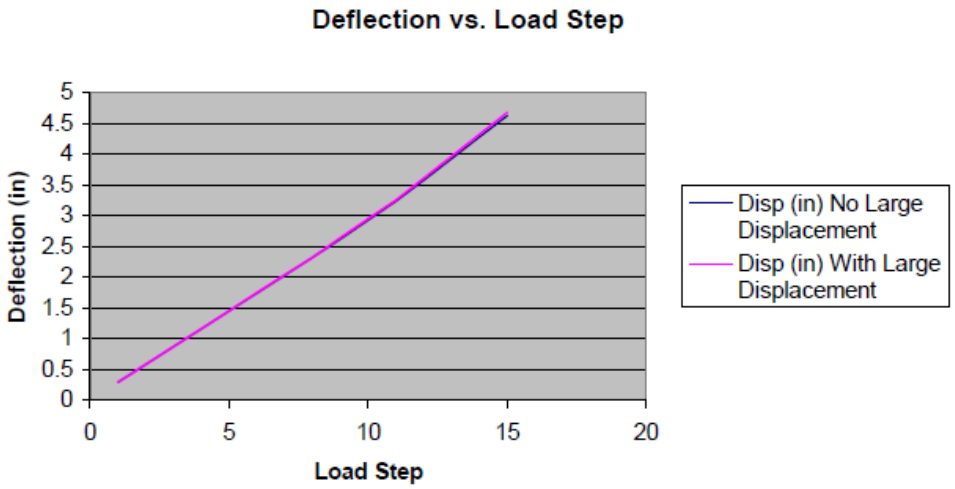

Figure 12. 2400 lb Load Case Deflection vs. Load Step

The yielding of the material begins at approximately load step 8 when the material stress reaches 34859 psi and a deflection of 2.32 in (Table 6 and Figure 12). Load step 8 is equivalent to an applied load of 8/15(2400 lbs) = 1280 lbs. This yields an equivalent spring constant of K = 1280 lbs/2.32 in = 552 lbs/ in. for the elastic portion of the deflection. Once the material begins to yield, the structure begins to deflect at a higher rate. The spring constant calculation for this portion of the deflection is calculated as K = (2400 lbs -1280 lbs)/(4.63 in-2.32 in) = 485 24 lbs/in. For the 2400 lb load case, the decrease in static resistance is only 13%. Figure 13 and Figure 14 show the stress distribution as the frame first approaches the yield point in step 8, and

as the frame approaches maximum deflection in step 15, while Figure 15 provides a section view of the stress distribution at the base of the frame at maximum deflection.

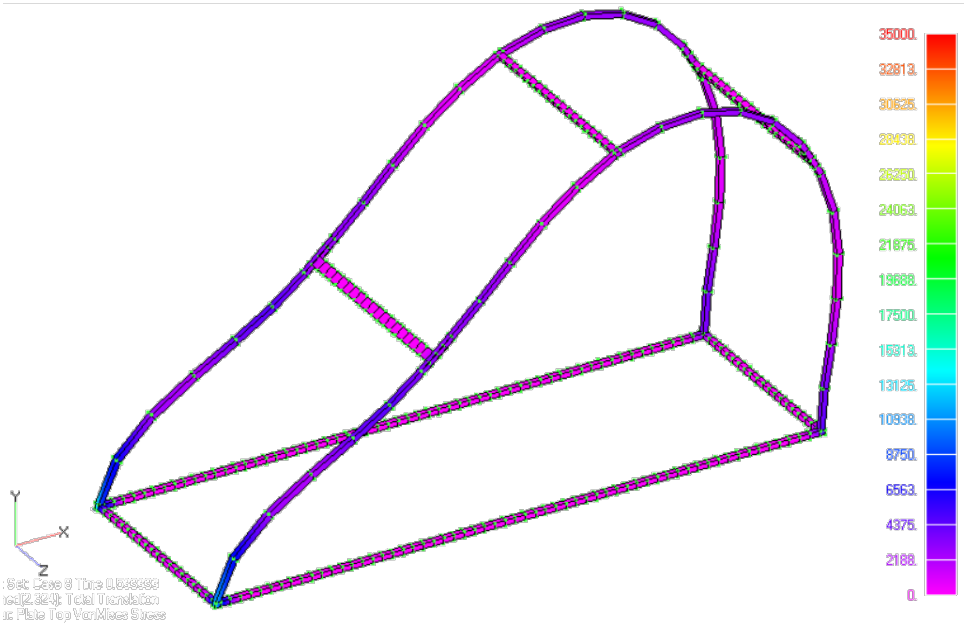

Figure 13. 2400 lb Load Case Yield Point

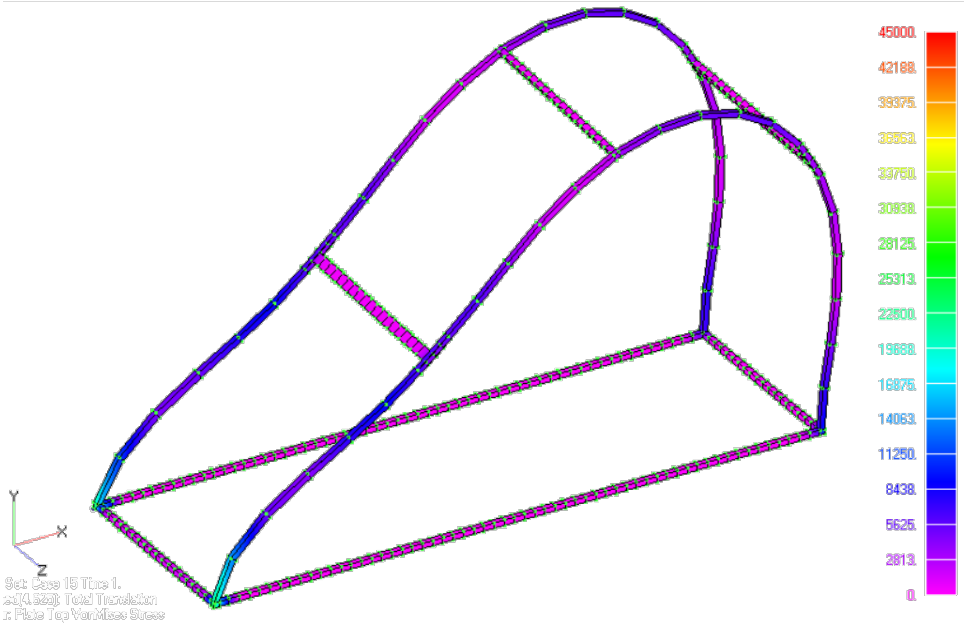

Figure 14. 2400 lb Load Case Maximum Deflection

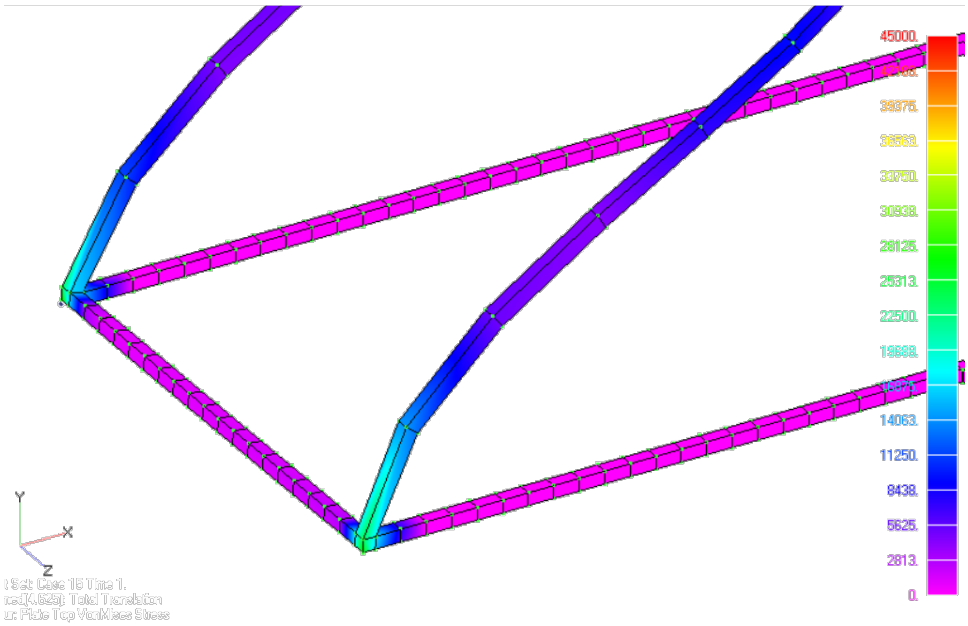

Figure 15. 2400 lb Load Case Maximum Deflection Section View

4.3.2. 4800 lb Load Case Results

Table 7 provides a summary of the maximum deflection at the selected nodes in the model for the 4800 lb load case. As shown in the figures and discussed previously for the 2400 lb load case, the difference in deflection due to the inclusion of large displacements is negligible when compared to the overall deflection of the system.

Table 7. 4800 lb Load Case Deflection

Load step	Node	No large displacements		Large displacements included	
		Displacement (in)	Stress (psi)	Displacement (in)	Stress (psi)
1	1097	0.58	8643	0.58	8663
2	1097	1.16	17288	1.16	17364
3	1097	1.75	25932	1.75	26100
4	1097	2.32	34576	2.33	34890
5	951	2.93	36938	2.95	37016
6	951	3.59	39757	3.62	39930
7	951	4.28	43473	4.33	43671
8	936	4.98	47276	5.04	47485
9	936	5.73	51370	5.80	51533
10	936	6.50	55566	6.58	55702
11	936	7.28	59706	7.37	59881
12	936	8.09	63467	8.18	63796
13	936	8.92	67034	9.00	67533
14	936	9.78	70672	9.83	71163
15	936	10.83	74780	10.73	75002

As shown previously, there is no difference in deflection until the material yield point is reached. Once the material yields, the deflection is greater for the analysis that includes large deflection effects, except for the last load step. The difference is once again negligible as it is only a change of 0.9%. Figure 16 provides a graph of the deflection versus load step overlaid for the analysis with large displacements turned both on and off.

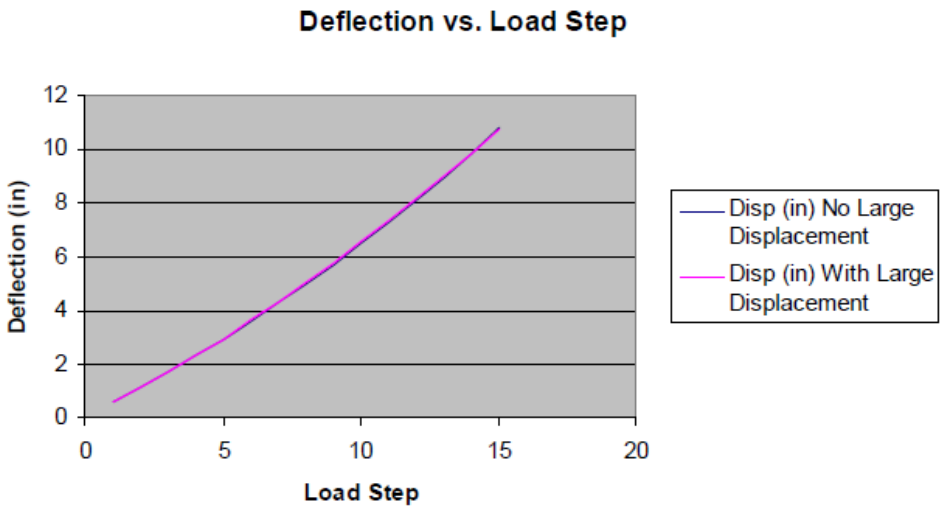

Figure 16. 4800 Load Case Deflection vs. Load Step

As can be seen from the above table and figure, yielding of the material begins at approximately load step 4 when the material stress reaches 34576 psi and a deflection of 2.32 in. Load step 4 is equivalent to an applied load of 4/15(4800 lbs) = 1280 lbs. This yields an equivalent spring constant of K = 1280 lbs/2.32 in =552 lbs/ in. for the elastic portion of the deflection. Once the material begins to yield, the structure begins to deflect at a higher rate. The spring constant calculation for this portion of the deflection is calculated as K = (4800 lbs -1280 lbs)/(10.83 in-2.32 in) = 414 lbs/in. For the 4800 lb load case, the decrease in static resistance is 25%. Figure 17 and Figure 18 show the stress distribution as the frame first approaches the yield point in step 4 and as the frame approaches maximum deflection in step 15. Figure 19 provides a section view of the stress distribution in step 15. This view provides a more detailed view of the stress distribution that clearly shows the maximum stress at the base 29 of the frame, with varying stress levels as the structure deflects in response to the distributed load.

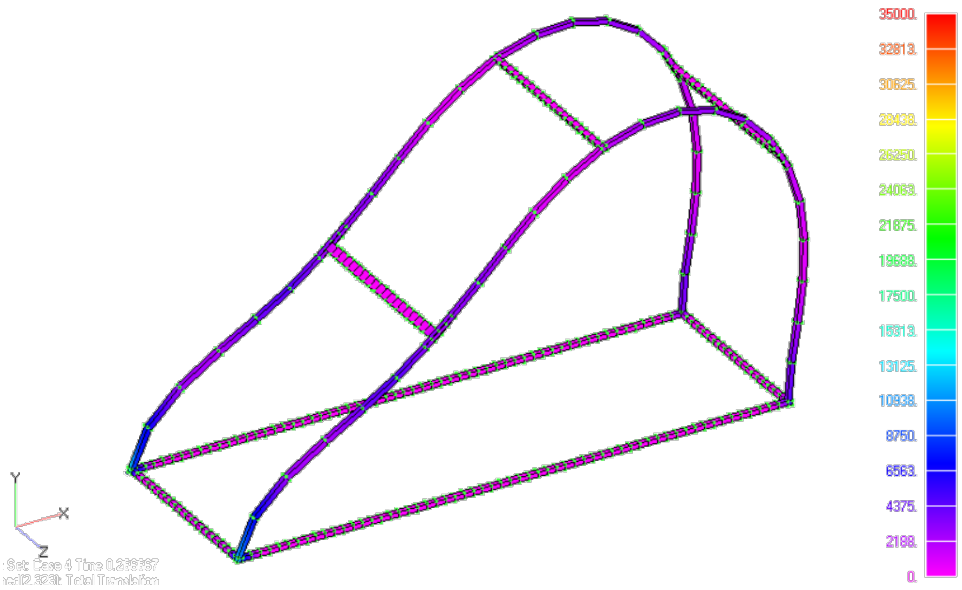

Figure 17. 4800 lb Load Case Yield Point

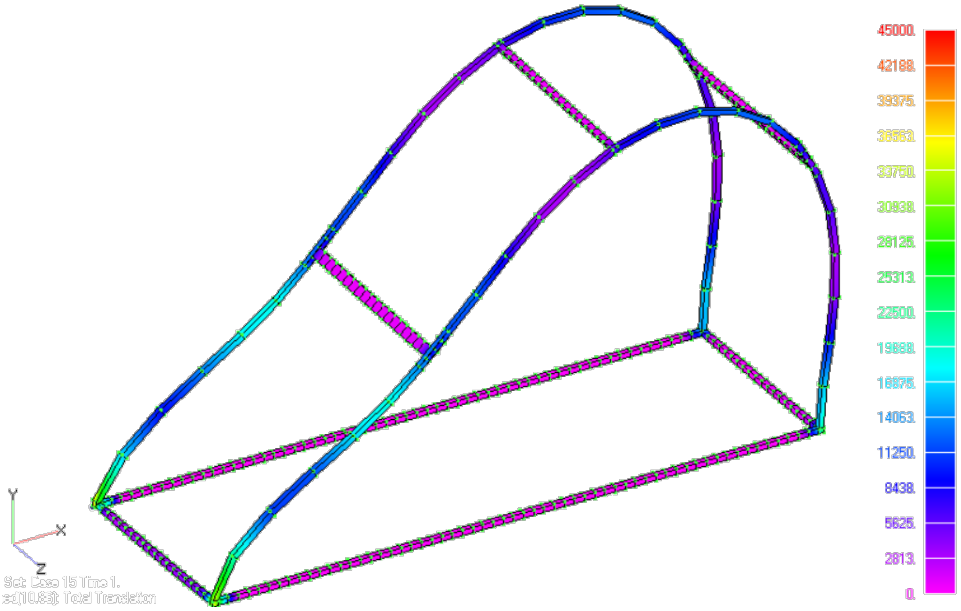

Figure 18. 4800 lb Load Case Maximum Deflection

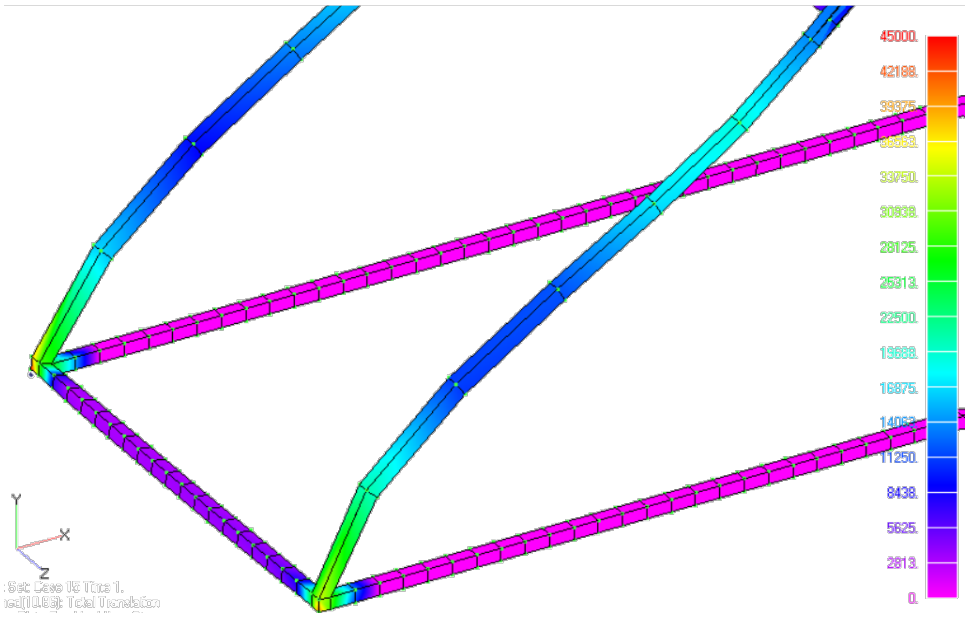

Figure 19. 4800 lb Load Case Maximum Deflection Section View

4.3.3. 7200 lb Load Case Results

Table 8 provides a summary of the maximum deflection at the selected nodes in the model for the 7200 lb load case. As shown in the figures and discussed previously for the 2400 lb and 4800 lb load cases, the difference in deflection due to the inclusion of large displacements is negligible when compared to the overall deflection of the system. There is no difference in deflection until the material yield point is reached. Once the material yields, the deflection is greater for the analysis that includes large deflection effects until approximately 10 in of deflection is reached, after that point, the analysis with no large displacement effects, i.e. no follower forces, produces the greater deflection. The difference is more noticeable for the 7200 lb analysis with a 5% difference in deflection. This large differential is attributed to the larger overall deflection, allowing for more impact due to the change in the applied force direction. Figure 20 provides a graph of the deflection versus load step overlaid for the analysis with large displacements turned both on and off.

Table 8. 7200 lb Load Case Deflection

Load step	Node	No large displacements		Large displacements included	
		Displacement (in)	Stress (psi)	Displacement (in)	Stress (psi)
1	1097	0.87	12956	0.87	12999
2	1097	1.74	25913	1.75	26081
3	951	2.62	35922	2.64	35997
4	951	3.58	39746	3.61	39920
5	936	4.62	45347	4.68	45554
6	936	5.73	51351	5.79	51514
7	936	6.88	57649	6.96	57783
8	936	8.09	63443	8.17	63771
9	936	9.33	68786	9.40	69325
10	936	10.82	74745	10.72	74965
11	936	12.60	81311	12.34	81314
12	936	14.43	88269	14.01	87828
13	936	16.29	95388	15.66	94506
14	936	18.27	102927	17.41	101532
15	936	20.49	111034	19.37	108937

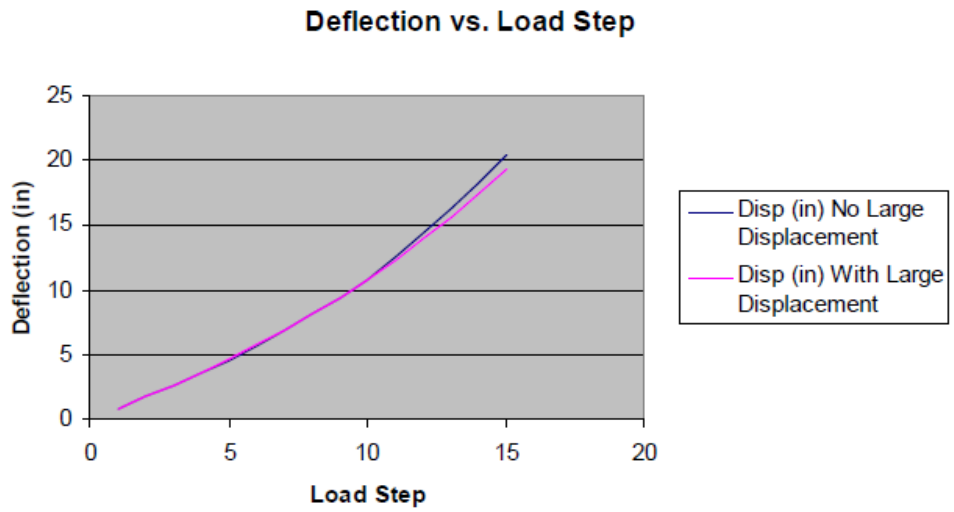

Figure 20. 4800 lb Load Case Deflection vs. Load Step

As can be seen from the above table and graph, yielding of the material begins at approximately load step 3 when the material stress reaches 35922 psi and a deflection of 2.62 in. Load step 3 is equivalent to an applied load of 3/15(7200 lbs) = 1440 lbs. This yields an equivalent spring constant of K = 1440 lbs/2.62 in = 550 lbs/ in. for the elastic portion of the deflection. Once the material begins to yield, the structure begins to deflect at a higher rate. The spring constant calculation for this portion of the deflection is calculated as K = (7200 lbs -1440 lbs)/(20.49 in-2.62 in) = 322 lbs/in. For the 7200 lb load case, the decrease in static resistance is 41%. Figure 21 and Figure 22 show the stress distribution as the frame first approaches the yield point in step 4, and as the frame approaches maximum deflection in step 15. Figure 23 also provides a section view of the stress distribution in step 15. This provides a more detailed view of the stress

distribution that clearly shows the maximum stress at the base of the 34 frame, with varying stress levels as the structure deflects in response to the distributed load.

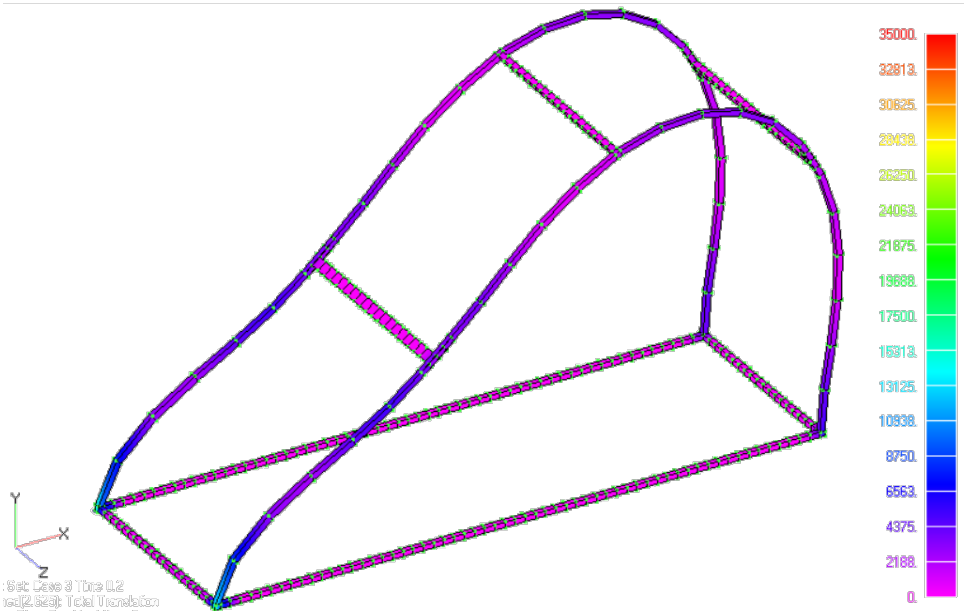

Figure 21. 7200 lb Load Case Yield Point

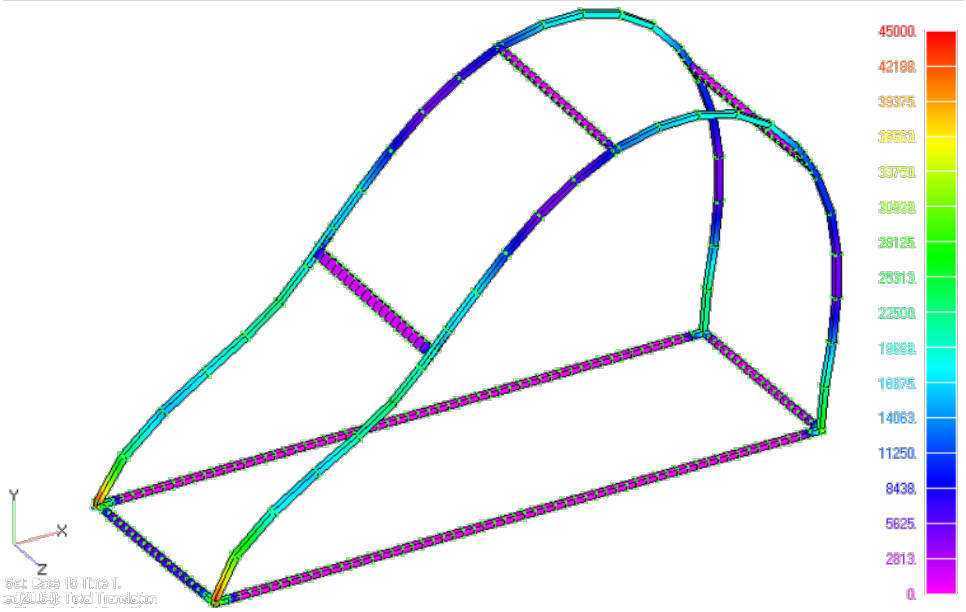

Figure 22. 7200 lb Load Case Maximum Deflection

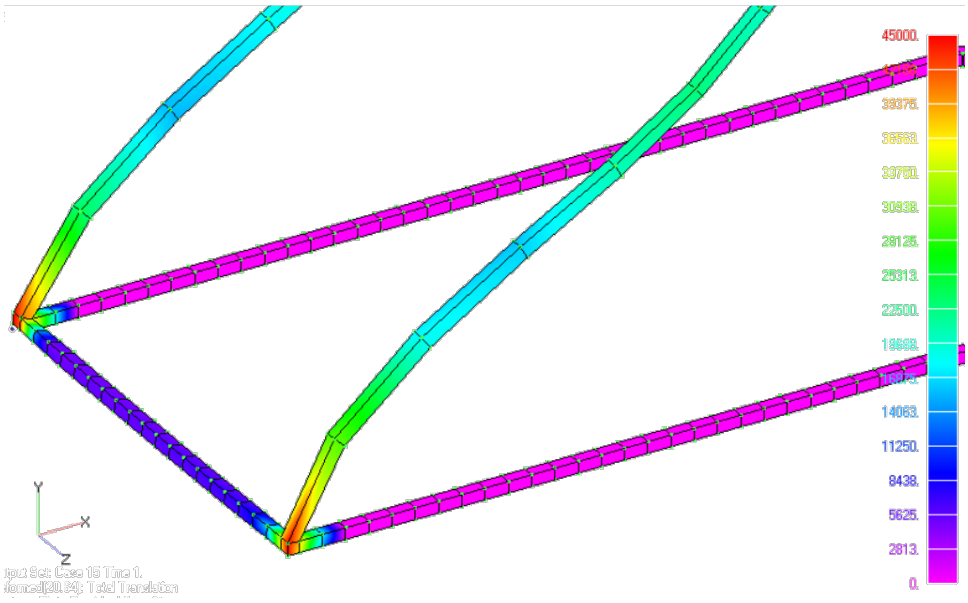

Figure 23. 7200 lb Load Case Maximum Deflection Section View

4.4. Analysis Parametric Study

The shelter field assembly provides a base support that is realistically somewhere between simply supported and fixed. All analysis in Section 4.3 assumed a fixed support. This section will repeat the analysis of the 2400 lb load case using a simply supported base to determine the impact of base restraint on the resistance function of the frame.

4.4.1. 2400 lb Load Case Results, Simply Supported

Table 9 provides a summary of the maximum deflection at the selected nodes in the model for the 2400 lb load case with a simply supported base. As in the fixed base condition, the difference in deflection due to the inclusion of large displacements is negligible when compared to the overall deflection of the system. Figure 24 provides a graph that includes an overlay of the displacements due to a 2400 lb load case with a fixed base and with a simply supported base. Large displacement effects were not included in these runs.

Table 9. 2400 lb Load Case Deflection, Simply Supported Base

Load step	Node	No large displacements		Large displacements included	
		Displacement (in)	Stress (psi)	Displacement (in)	Stress (psi)
1	1097	0.29	4330	0.29	4335
2	1097	0.58	8661	0.58	8680
3	1097	0.87	12991	0.87	13034
4	1097	1.16	17321	1.16	17397
5	1097	1.45	21652	1.45	21769
6	1097	1.74	25982	1.75	26150
7	1097	2.03	30313	2.04	30540
8	1097	2.32	34643	2.33	35009
9	951	2.62	35953	2.64	36027
10	951	2.93	36970	2.95	37048
11	951	3.24	38003	3.27	38163
12	951	3.59	39827	3.62	40001
13	951	3.94	41691	3.97	41878
14	951	4.28	43581	4.33	43779
15	951	4.63	45489	4.68	45695

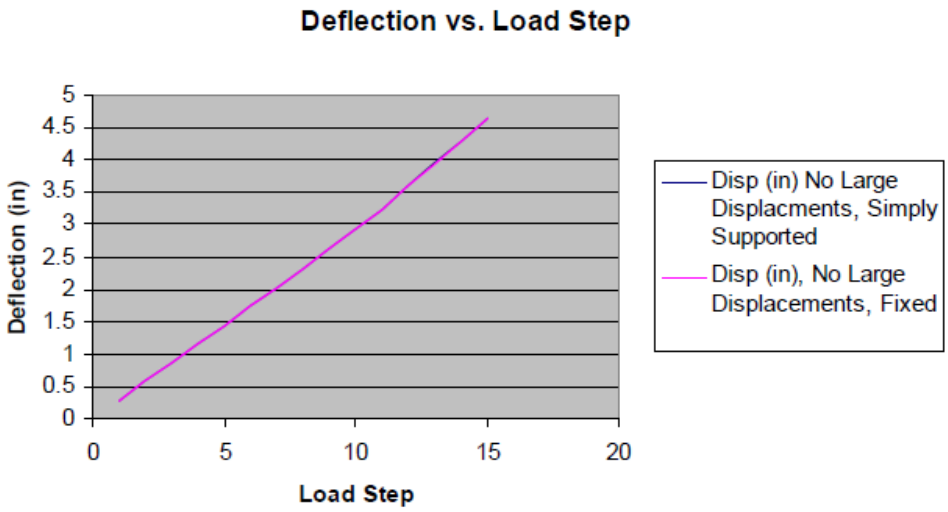

Figure 24. 2400 lb Load Case Deflection vs. Load Step

As seen in Figure 24, the base support condition has no appreciable impact on the deflection and stress distribution; therefore, the static resistance function developed using the fixed base condition is valid even when considering the uncertainty of the actual base restraint condition.

4.5. Static Resistance Function

The three load cases discussed in the previous sections provide a foundation to develop a static resistance function that could be used in a SDOF Model to predict the deflection of the frame subjected to impulse loading. The function will need to consist of a piecewise linear

representation of the frame stiffness with the curve defining the stiffness through the elastic and plastic material phase as well as accounting for the effects of large displacement.

4.5.1. Elastic Static Resistance Function

The elastic portion of the curve was consistent among the three load case analysis performed. Each load case showed that the material begins to yield at approximately 1300 lbs of applied force. Table 10 provides a summary of the three load cases, along with maximum material stress, displacement, and the resulting stiffness calculation.

Table 10. Elastic Stiffness Summary

Load case	Load step	Stress (psi)	Load at yield (lbs)	Displacement (in)	Stiffness (lb/in)
2400 lbs	8	34554	1280	2.32	552
4800 lbs	4	34576	1280	2.32	552
7200 lbs	3	35922	1440	2.62	550

The above cases show good correlation among the three load cases analyzed and provide an elastic stiffness of 550 lbs/in until a deflection of 2.3 in is reached.

4.5.2. Plastic Static Resistance Function

Analysis of the frame model at the material yield point and beyond shows that the stiffness of the structure continues to decrease as the deflection increases. Even though the material stress versus strain curve is linear before and after the yield point, the apparent stiffness continues to decrease due to the deflection of the structure and the resulting recalculation of the stiffness matrix in the NASTRAN model based on the updated geometry. Therefore, two plastic stiffness numbers will be used for the plastic portion of the curve. The first portion will be based on the deflection of all three load cases and will encompass the stiffness up to a deflection of approximately 4.6 in, which is the maximum deflection found in the 2400 lb load case. Table 11 provides a summary for all three load cases up to the 4.6 in deflection. Data from all three load cases is included in the table, even though interpolation is required to correlate the data for the 4800 lb load case, since the nearest deflections are at 4.3 in and 5.0 in.

Table 11. Initial Plastic Stiffness Summary

Load case	Load step	Stress (psi)	Load (lbs)	Displacement (in)	Stiffness (lb/in)
2400 lbs	15	45340	2400	4.63	485
4800 lbs	7 and 8	45374	2400	4.65	481
7200 lbs	5	45374	2400	4362	480

The calculation of the stiffness using the data above is shown in the following equations.

2400 lb load case K = (2400 lbs-1280 lbs)/(4.63 in-2.32 in)
4800 lb load case K = (2400 lbs-1280 lbs)/(4.65 in-2.32 in)
7200 lb load case K = (2400 lbs-1440 lbs)/(4.62 in-2.62 in)

Table 11 shows that the minor variations in the point at which the material yield point is assumed to be reached do not influence the calculation.

The second portion of the plastic stiffness calculation will be based on deflection data from the 4800 lb and 7200 lb load cases. This calculation will encompass the stiffness up to a deflection of 10.83 in, which is the maximum deflection found in the 4800 lb load case. Table 12 provides a summary of data for the stiffness calculation for the second portion of the plastic curve.

Table 12. Second Plastic Stiffness Summary

Load Case	Load Step	Stress (psi)	Load at Yield (lbs)	Displacement (in)	Stiffness (lb/in)
4800 lbs	15	74780	4800	10.83	387
7200 lbs	10	74745	4800	10.82	387

The calculation of the stiffness using the data above is shown in the following equations.

4800 lb load case K = (4800 lbs-2400 lbs)/(10.83 in-4.63 in)
7200 lb load case K = (4800 lbs-2400 lbs)/(10.82 in-4.63 in)

4.5.3. Static Resistance Function Development

The three stiffness values for the various deflections are assembled into one curve, shown in Figure 25, which represents the static resistance function for the frame. This curve is incorporated into a SDOF model of the frame that represents the applied load, stiffness, and mass of the structure.

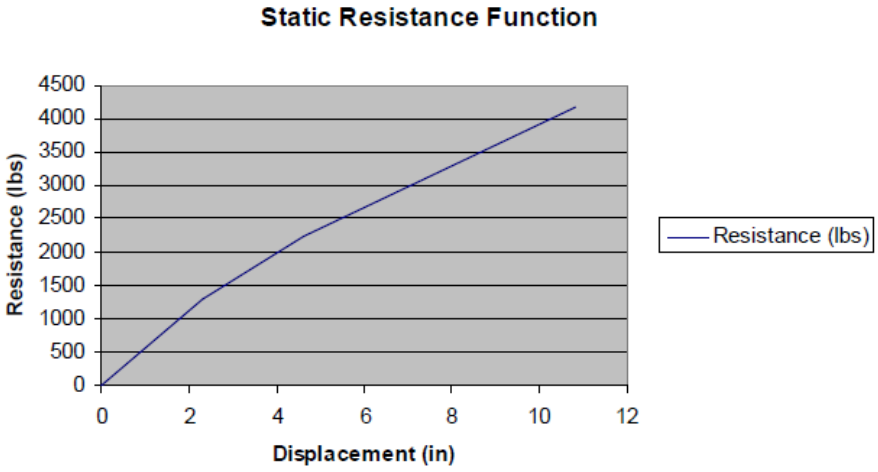

Figure 25. Static Resistance Function

5. LS-DYNA IMPULSE LOAD SIMULATION RESULTS

The results of the effort to validate the predictive capability of LS-DYNA impulse load modeling applied to the aluminum arch frames are summarized in Table 13. The correlation between the model results and test data shows a significant lack of agreement, primarily due to two significant differences between the test cases and the analytical models. The first difference is that the load application in the test cases is applied to the entire shelter structure including fabric; while in the analytical models, only the exposed aluminum structure is considered for load application. The second difference is due to the lack of the fabric weight and stiffness in the analytical models.

In addition to the test case results, four additional cases were modeled to simulate points along the pressure-impulse diagram that is documented in the test report. The correlation for these cases showed the same lack of agreement between the predicted results and the model results for the four conditions chosen. The four conditions were chosen to follow the pressure-impulse diagram, with two cases falling on the minor to no damage portion of the curve, and the other two cases falling on the severe to failure portion of the curve. As described in Section 4, all deflections were taken from the interface of the purlin to the arch on the side facing the impulse load. The model recovery point is shown in Figure 26. The deflections for this point are typical for purlin deflections on either side of the frame. The following sections present the results of each analysis including graphs of deflection versus time for each load case and maximum stress within the aluminum arch.

Table 13. Model Impulse Analysis Results

Reflected Impulse (psi-ms)	Displacement (in)	Model Predicted Result	Test Damage Level	Prediction Curve **
81.1	4.3	Minor	Severe	Failure
55.7	3.5	None	Minor	Moderate
30.5	3.5	None	None	Minor
94.8	10.1	Minor	Severe	Failure
76.4	8.5	Minor	Severe	Severe
55.0	6.0	Minor	Minor	Minor
32.2	3.4	None	None	Threshold
111.0	6.8	Minor	N/A	Failure
24.7	3.1	None	N/A	Minor
116.8	8.0	Minor	N/A	Failure
33.1	4.0	Minor	N/A	Minor

**Utilizing the reduced impulse curve presented in the test report

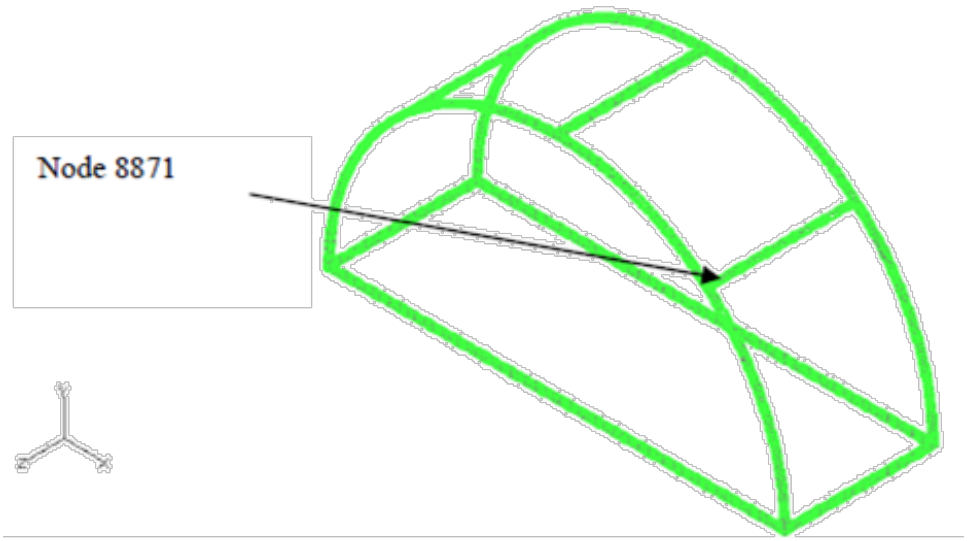

Figure 26. Deflection Recovery Node

5.1. 81.1 psi-ms Results

Results for this load case are shown in Figure 27 and Figure 28. Maximum deflection was approximately 4.3 in, which falls on the threshold of minor damage (Figure 27). The model was terminated after two complete cycles of the frame. In addition, the maximum stress at the base of the arch did not exceed the yield stress of the arch material (Figure 29). The lack of material yield with the 4.6 in deflection is a lack of correlation with the resistance function that can be seen in several of the following load cases. This difference is primarily due to the deflected shape providing higher deflections at the purlin for some blast cases.

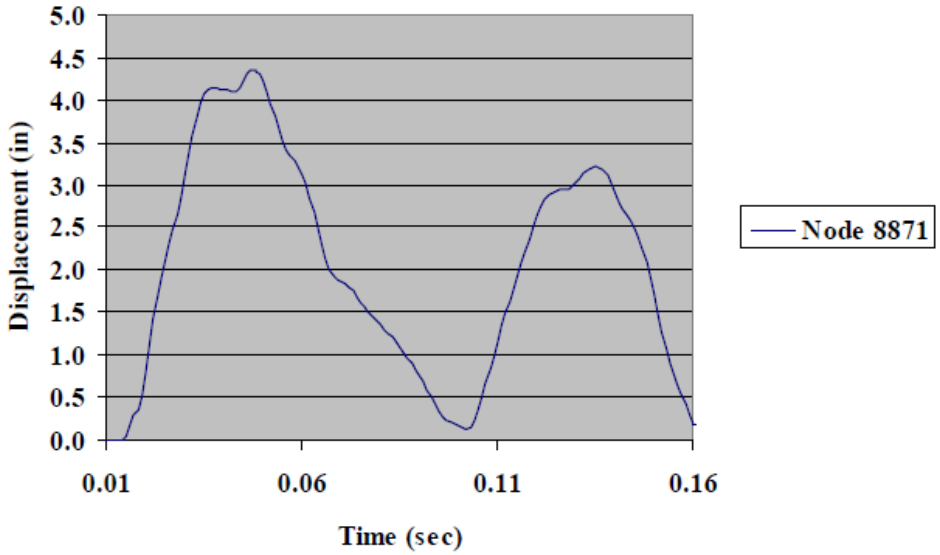

Figure 27. Purlin Translation for 81.1 psi-ms

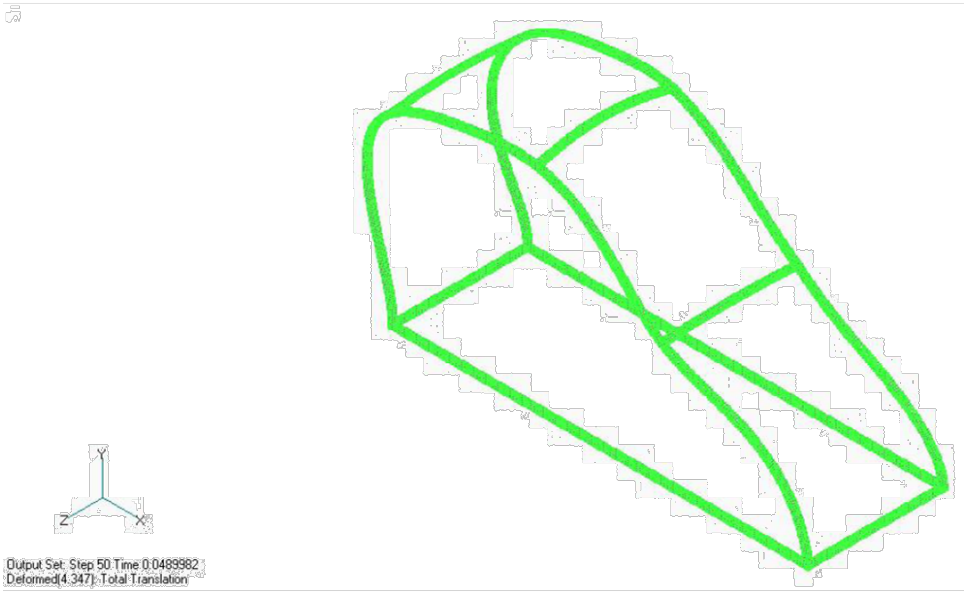

Figure 28. Arch Deflected Shape for 81.1 psi-ms

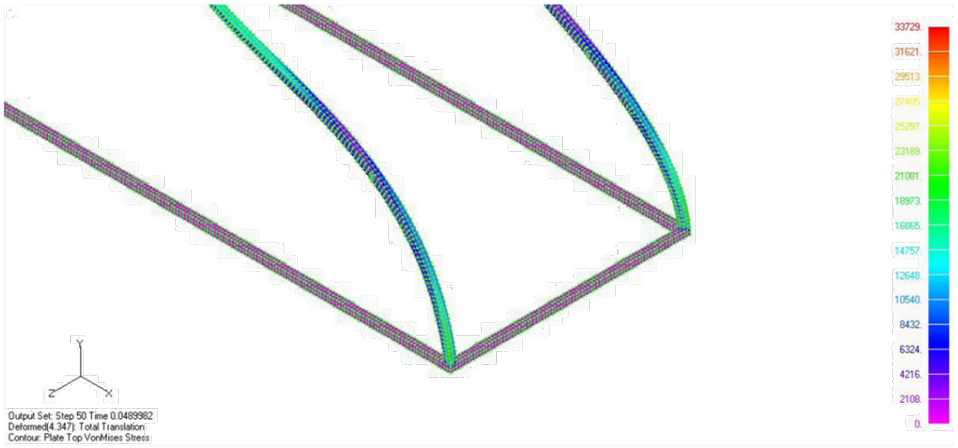

Figure 29. Arch Stress Distribution for 81.1 psi-ms

5.2. 55.7 psi-ms Results

Results for this load case are shown in Figure 30 and Figure 31. Maximum deflection was approximately 3.5 in, which falls in the minor to no damage category (Figure 30). Figure 31 provides a deformed view of the structure. In addition, the maximum stress did not exceed the material yield stress, as shown in Figure 32.

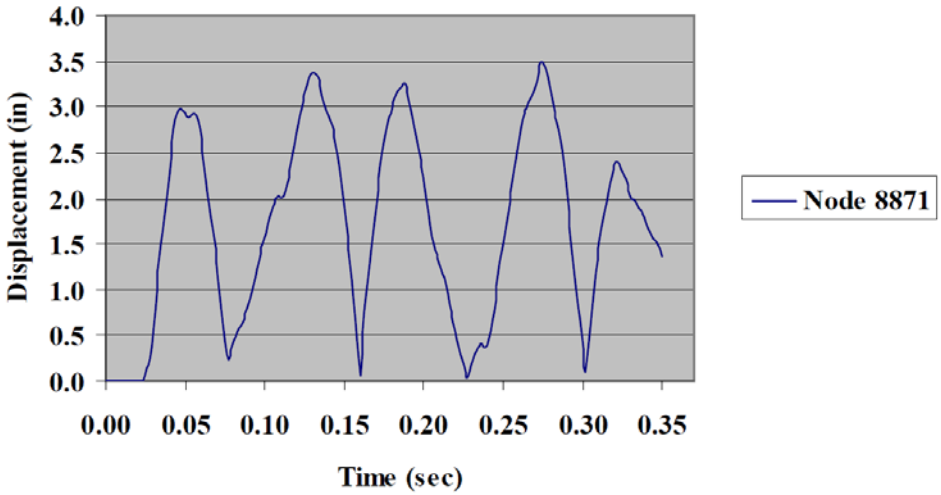

Figure 30. Purlin Translation for 55.7 psi-ms

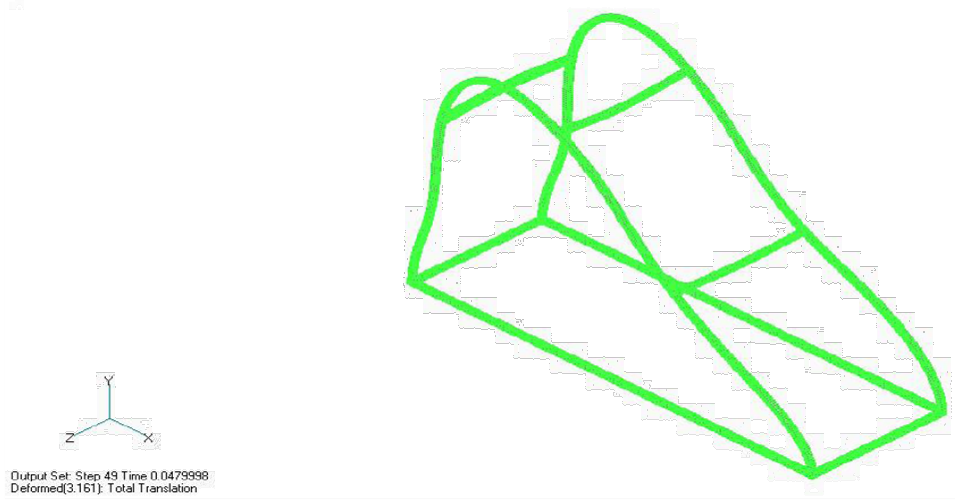

Figure 31. Arch Deflected Shape for 55.7 psi-ms

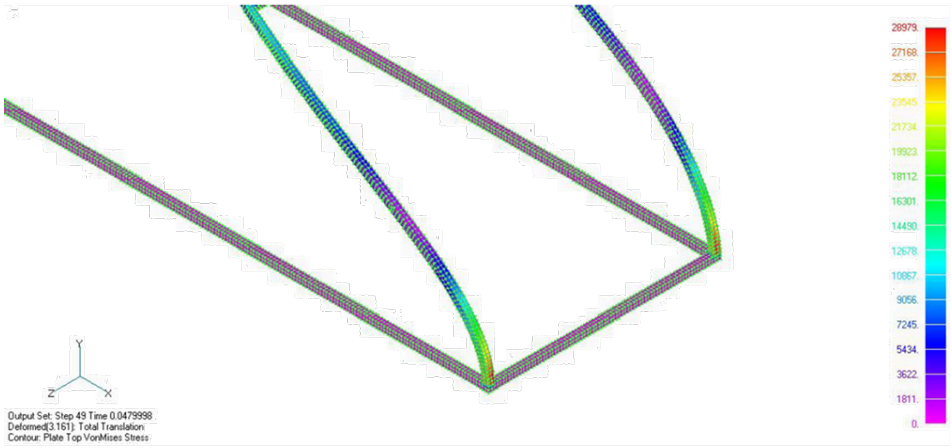

Figure 32. Arch Stress Distribution for 55.7 psi-ms

5.3. 30.5 psi-ms Results

Results for this load case are shown in Figure 33 and Figure 34. Maximum deflection was approximately 3.5 in, which falls in the minor to no damage category and correlates with the damage that was reported from the actual test result (Figure 33). Figure 34 provides an image of the deformed shape of the structure at approximately 1.8 in of purlin deflection, while Figure 35 provides a stress contour of the structure at approximately 1.8 in of deflection, which corresponds to the maximum deflection for the first peak of the deflection curve. The maximum stress at the base of the structure did not exceed the material yield stress (Figure 35).

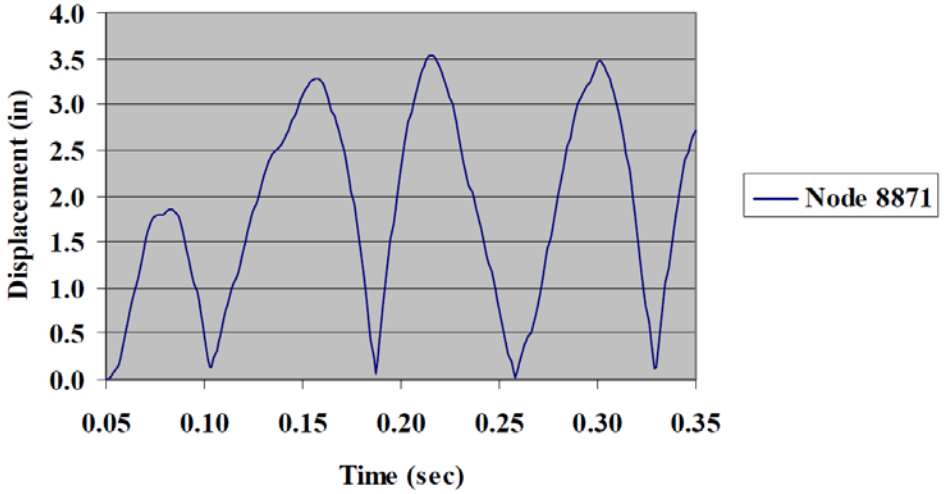

Figure 33. Purlin Translation for 30.5 psi-ms

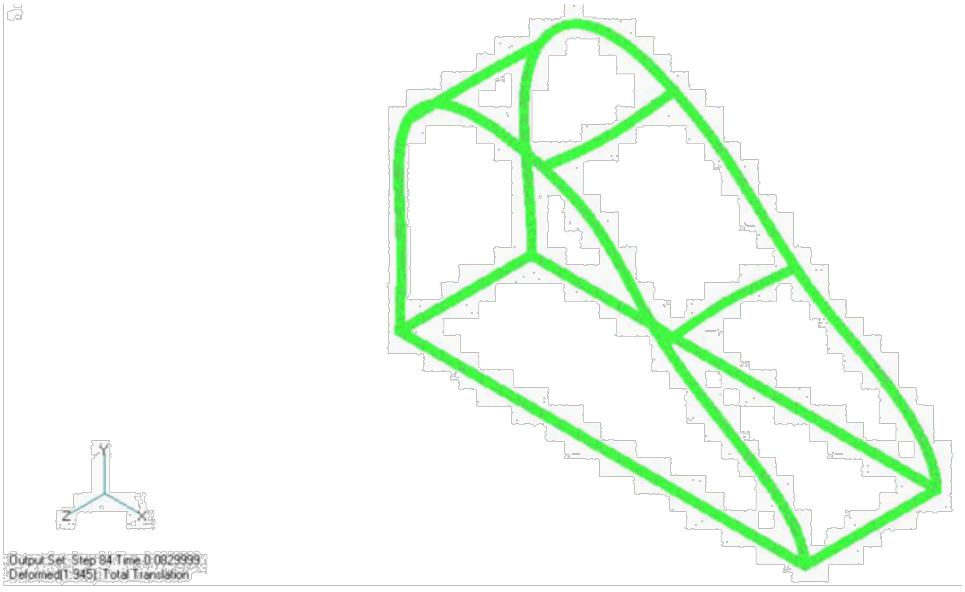

Figure 34. Arch Deflected Shape for 30.5 psi-ms

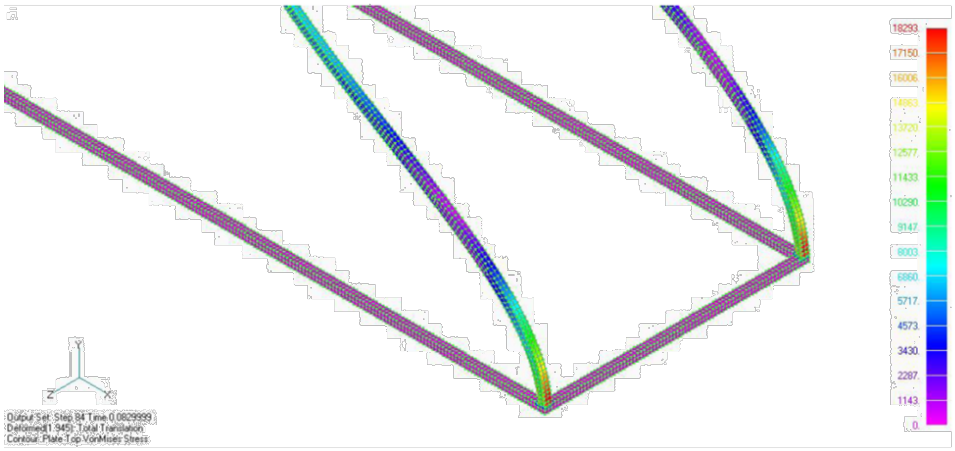

Figure 35. Arch Stress Distribution for 30.5 psi-ms

5.4. 94.8 psi-ms Results

Results for this load case are shown in Figure 36 and Figure 37. Maximum deflection in the structure was 10.1 in, which falls in the minor damage category and does not agree with the test report prediction curve (Figure 36). However, the predicted damage for this case is high in the minor category and is nearing the severe category. Figure 37 provides an image of the deformed shape of the structure at approximately 6.8 in of purlin deflection while Figure 38 provides a stress contour of the structure at approximately 6.8 in of deflection, which corresponds to the maximum deflection for the first peak of the deflection curve. The maximum stress at the base of the structure exceeds the material yield stress (Figure 38).

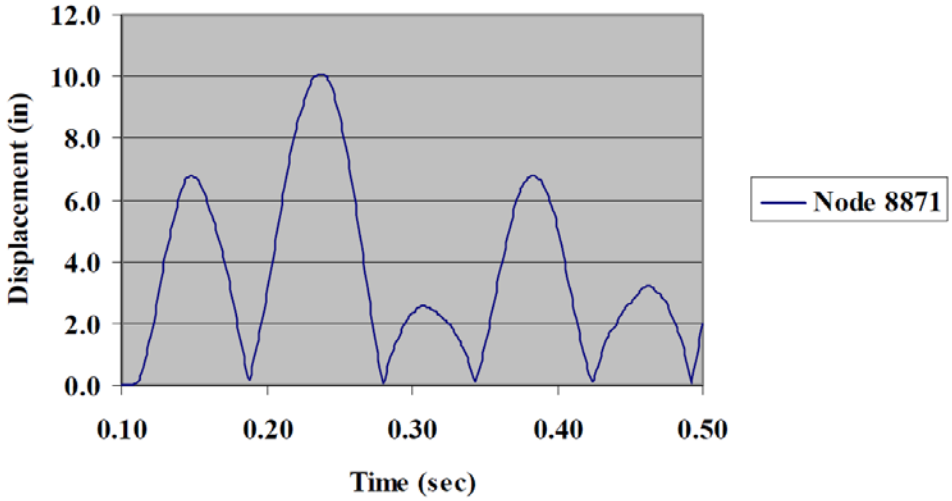

Figure 36. Purlin Translation for 94.8 psi-ms

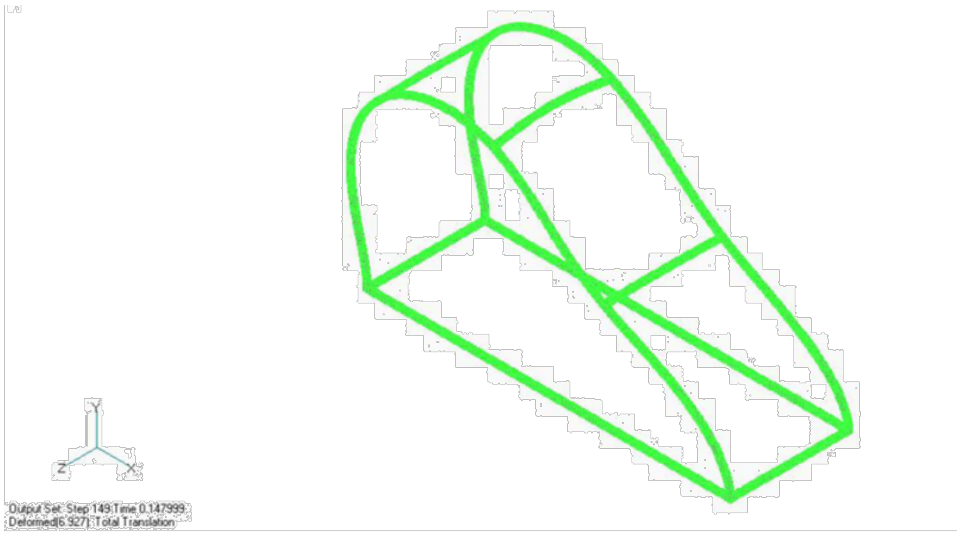

Figure 37. Arch Deflected Shape for 94.8 psi-ms

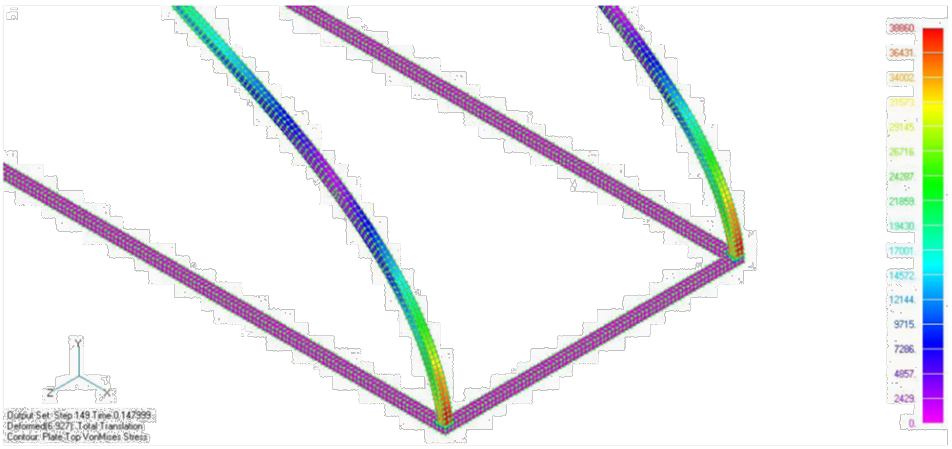

Figure 38. Arch Stress Distribution for 94.8 psi-ms

5.5. 76.4 psi-ms Results

Results for this load case are shown in Figure 39 and Figure 40. Maximum deflection in the structure was approximately 8.5 in, which falls in the minor damage category and is below the damage predicted by the test report curve (Figure 39). Figure 40 provides an image of the deformed shape of the structure at approximately 5.4 in of purlin deflection, while Figure 41 provides a stress contour of the structure at approximately 5.4 in of deflection, which corresponds to the maximum deflection for the first peak of the deflection curve. The maximum stress at the base of the structure equals the material yield stress (Figure 41).

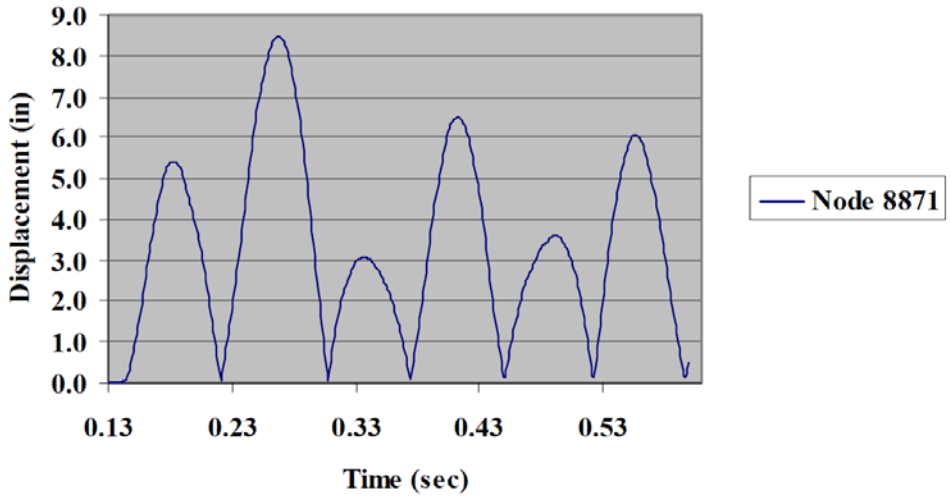

Figure 39. Purlin Translation for 76.4 psi-ms

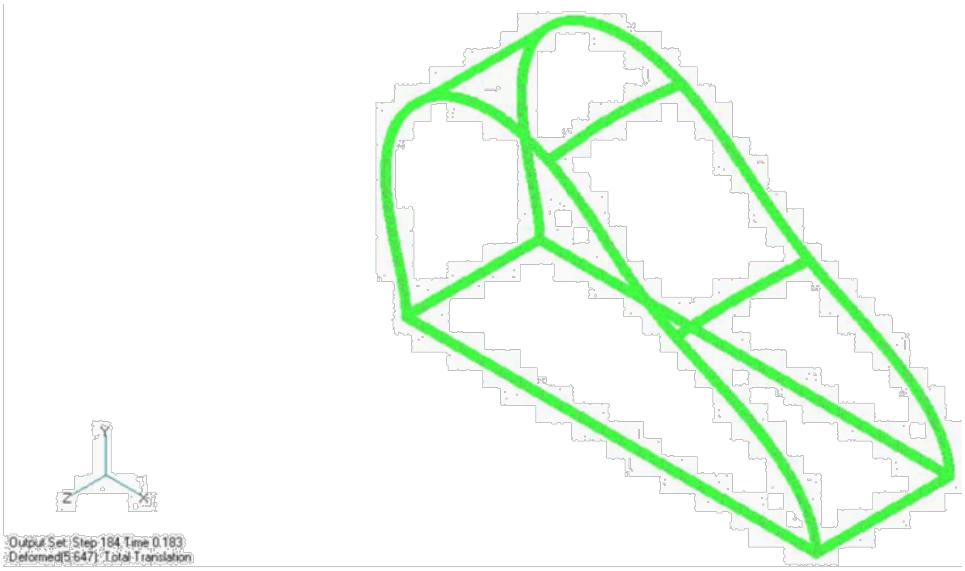

Figure 40. Arch Deflected Shape for 76.4 psi-ms

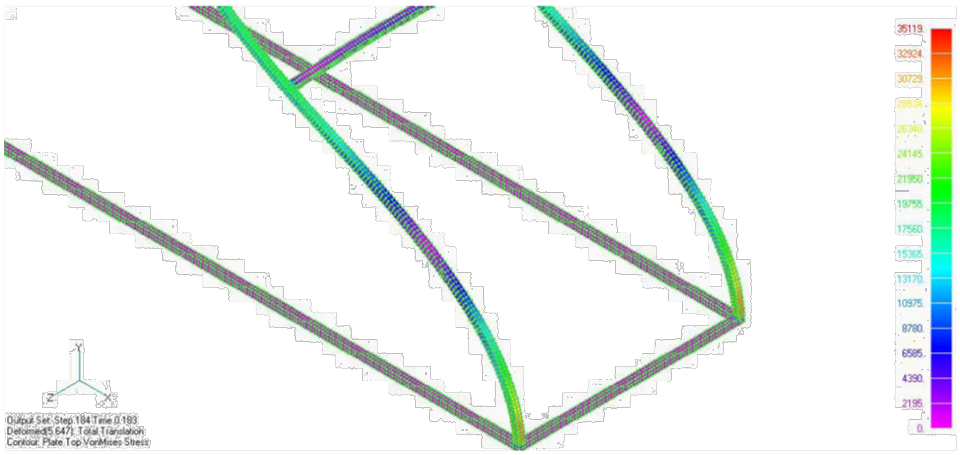

Figure 41. Arch Stress Distribution for 76.4 psi-ms

5.6. 55.0 psi-ms Results

Results for this load case are shown in Figure 42 and Figure 43. Maximum deflection in the structure was approximately 6.0 in, which falls in the minor damage category and correlates to the damage predicted by the test report curve (Figure 42). Figure 43 provides an image of the deformed shape of the structure at approximately 3.9 in of purlin deflection, while Figure 44 provides a stress contour of the structure at approximately 3.9 in of deflection, which corresponds to the maximum deflection for the first peak of the deflection curve. The maximum stress at the base of the structure is less than the material yield stress (Figure 44).

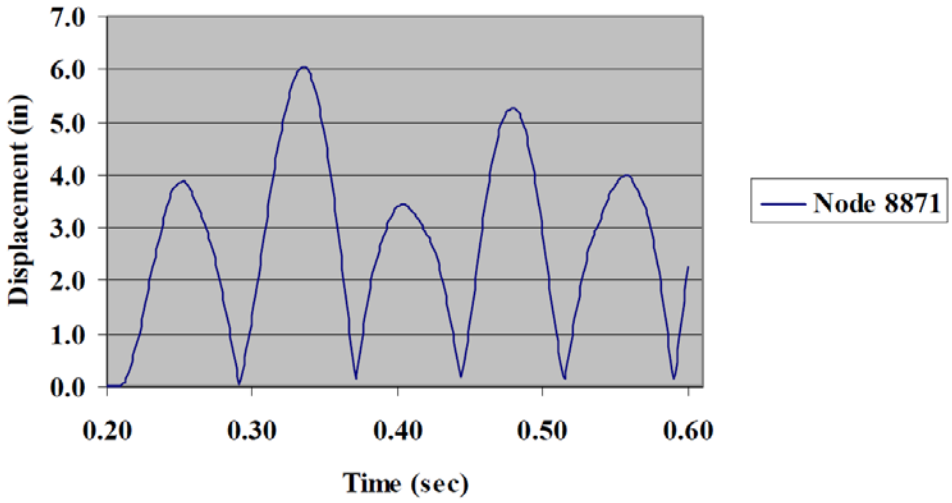

Figure 42. Purlin Translation for 55.0 psi-ms

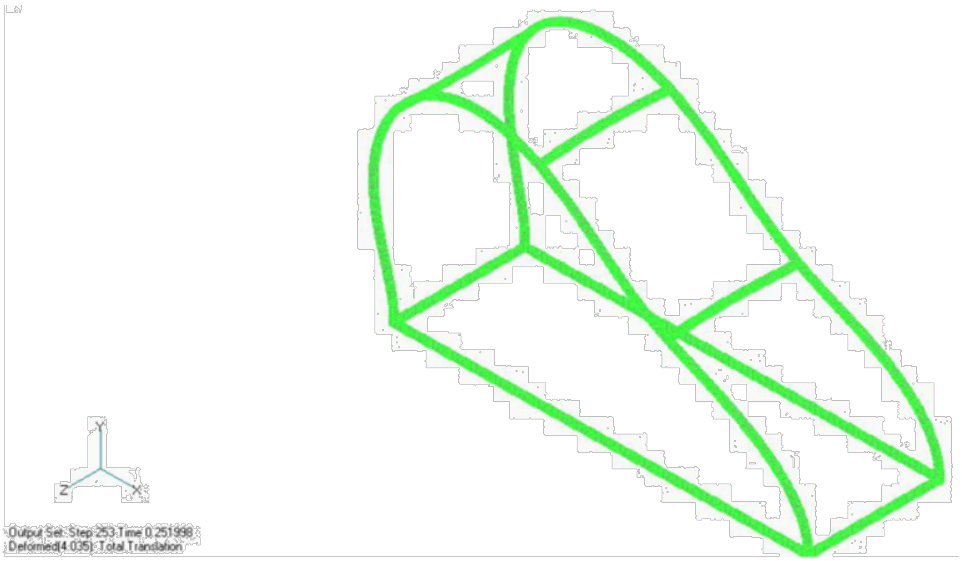

Figure 43. Arch Deflected Shape for 55.0 psi-ms

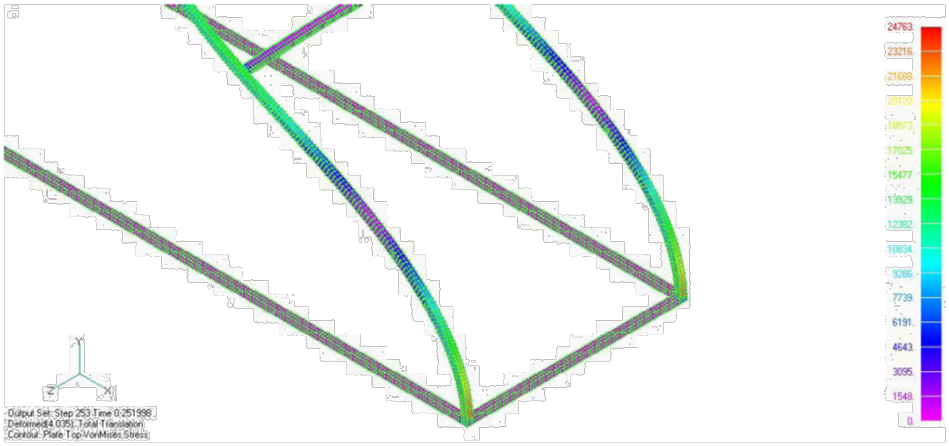

Figure 44. Arch Stress Distribution for 55.0 psi-ms

5.7. 32.2 psi-ms Results

Results for this load case are shown in Figure 45 and Figure 46. Maximum deflection in the structure was approximately 3.4 in, which falls in the no damage category and is slightly below the result presented in the test report and in line with the damage predicted by the test report curve presented (Figure 45). Figure 46 provides an image of the deformed shape of the structure at approximately 2.2 in of purlin deflection, while Figure 47 provides a stress contour of the structure at approximately 2.2 in of deflection, which corresponds to the maximum deflection for the first peak of the deflection curve. The maximum stress at the base of the structure is less than the material yield stress (Figure 47).

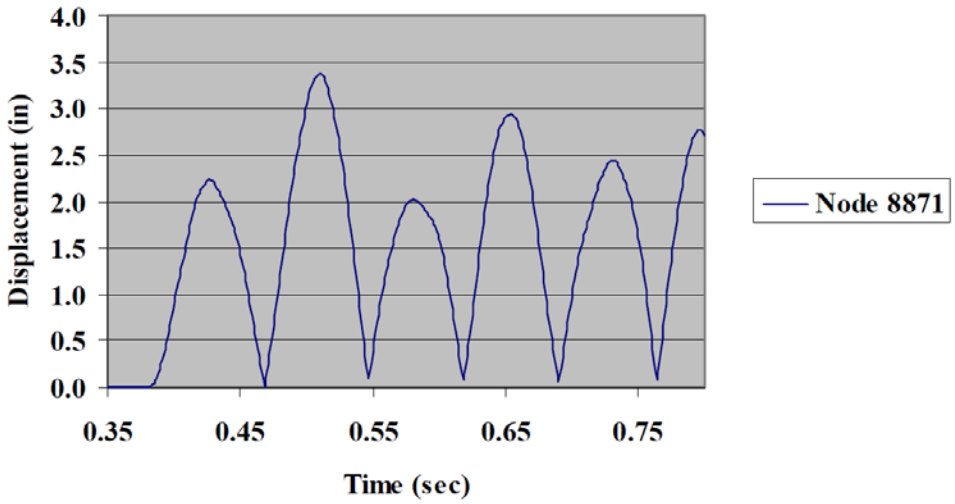

Figure 45. Purlin Translation for 32.2 psi-ms

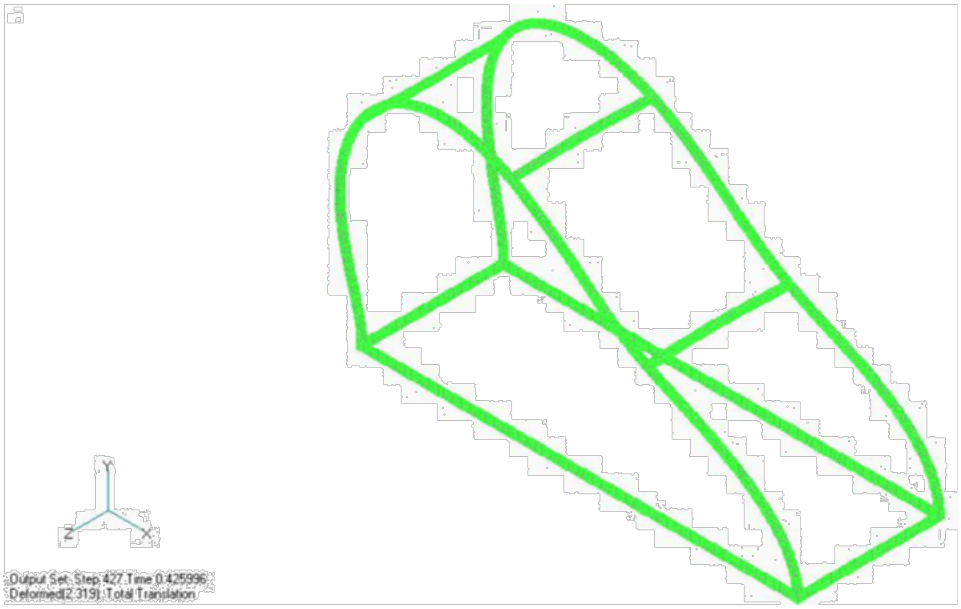

Figure 46. Arch Deflected Shape for 32.2 psi-ms

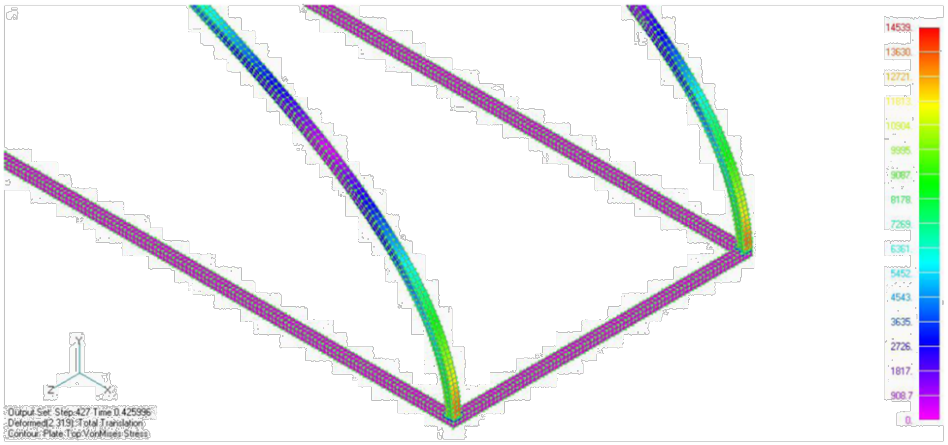

Figure 47. Arch Stress Distribution for 32.2 psi-ms

5.8. 111.0 psi-ms Results

Results for this load case are shown in Figure 48 and Figure 49. This load was chosen to represent an impulse load that should fall into the failure mode when one uses the test report prediction curve. Maximum deflection in the structure was approximately 6.8 in, which falls in the minor damage category and is below the damage predicted by the test report curve (Figure 48). Figure 49 provides an image of the deformed structure at maximum deflection, while Figure 50 provides a stress contour of the base of the structure at maximum deflection. The maximum stress in the structure does exceed the material yield stress (Figure 50).

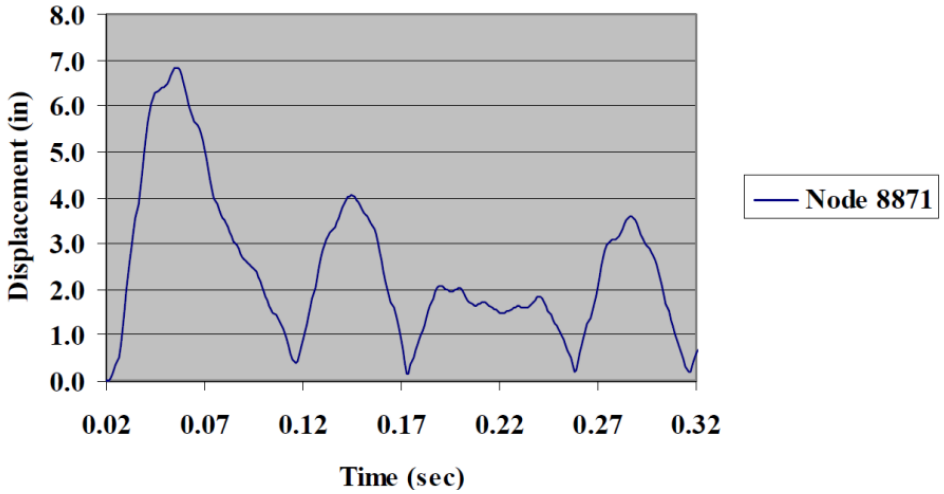

Figure 48. Purlin Translation for 111.0 psi-ms

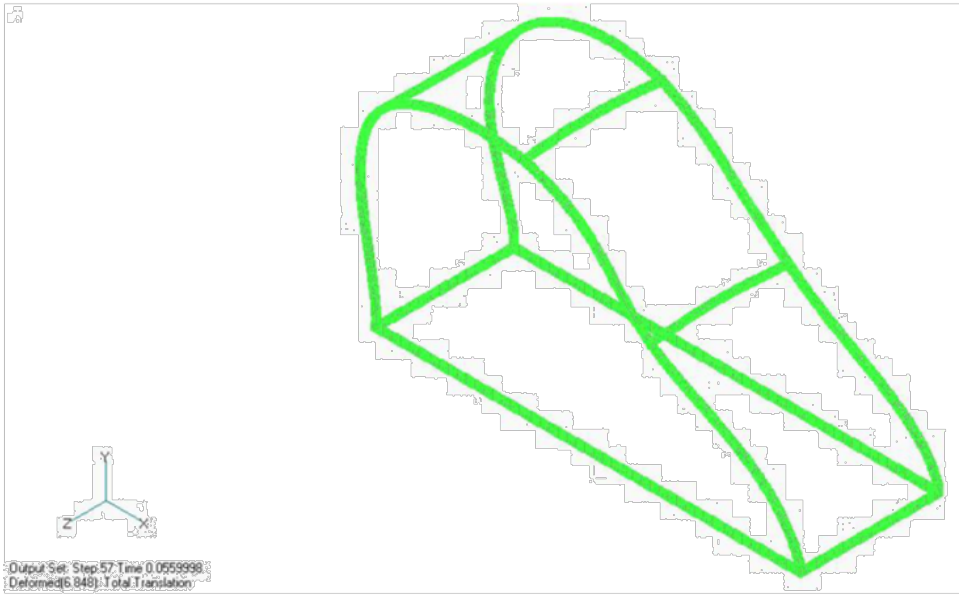

Figure 49. Arch Deflected Shape for 111.0 psi-ms

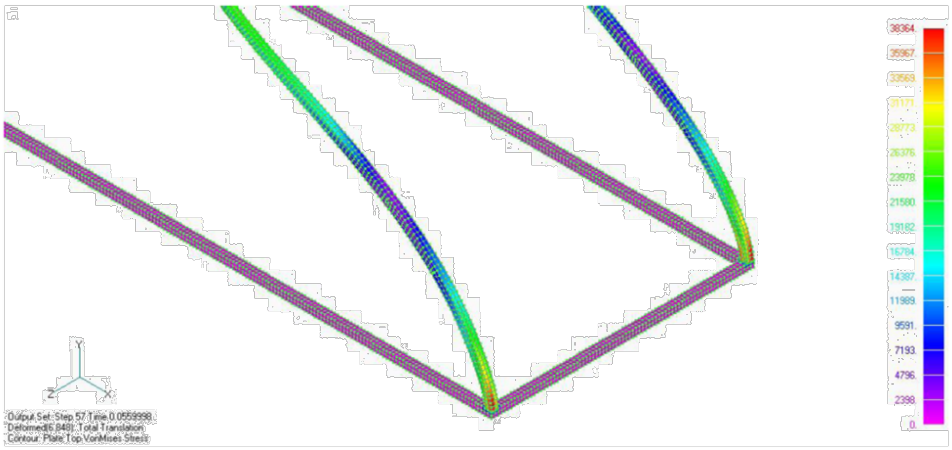

Figure 50. Arch Stress Distribution for 111.0 psi-ms

5.9. 24.7 psi-ms Results

Results for this load case are shown in Figure 51 and Figure 52. This load was chosen to represent an impulse load that should fall into the minor damage region when using the test report prediction curve. As shown in Figure 51, maximum deflection in the structure was approximately 3.1 in, which falls in the no damage category and is in line with the damage predicted by the test report curve, since the cutoff between no damage and minor damage is 4.0 in. Figure 52 provides an image of the deformed shape of the structure at approximately 1.7 in of purlin deflection, while Figure 53 provides a stress contour of the structure at approximately 1.7 in of deflection, which corresponds to the maximum deflection for the first peak of the deflection curve. As can be seen in Figure 53, the maximum stress at the base of the structure is less than the material yield stress

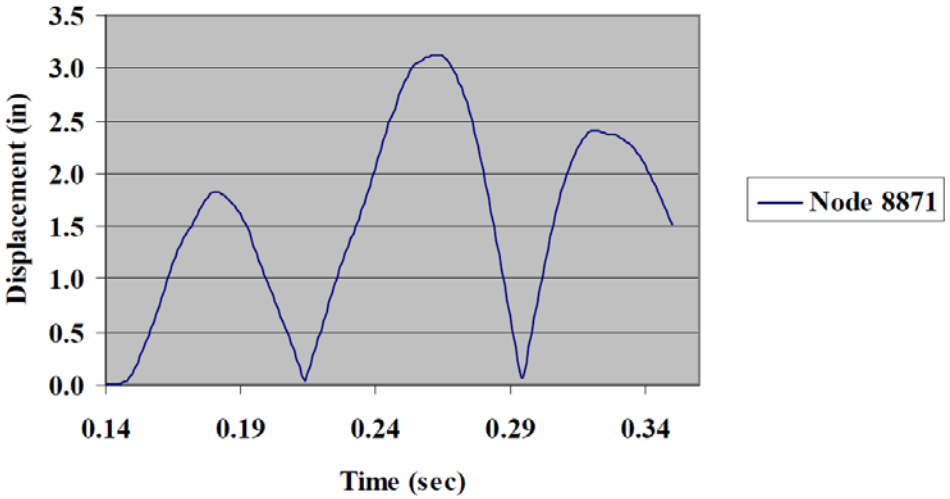

Figure 51. Purlin Translation for 24.7 psi-ms

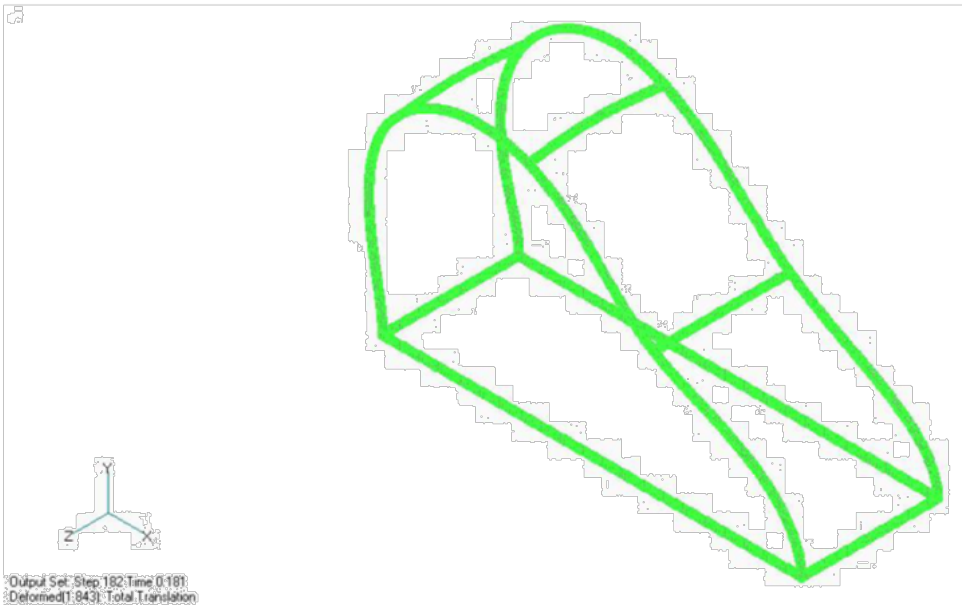

Figure 52. Arch Deflected Shape for 24.7 psi-ms

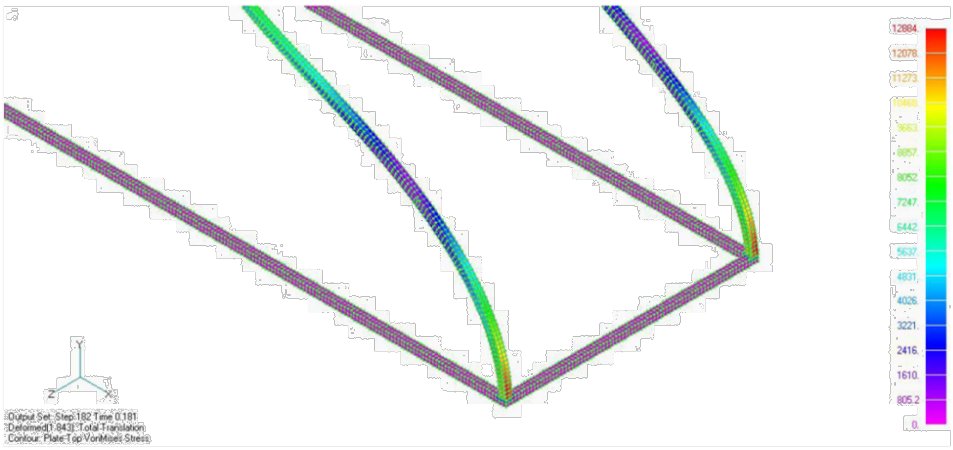

Figure 53. Arch Stress Distribution for 24.7 psi-ms

5.10. 116.8 psi-ms Results

Results for this load case are shown in Figure 54 and Figure 55. This load was chosen to represent an impulse load that should fall into the failure mode when utilizing the test report prediction curve. Maximum deflection in the structure was approximately 8.0 in, which falls in the minor damage category and is less than the damage predicted by the test report curve (Figure 54). Figure 55 provides an image of the deformed structure at maximum deflection, while Figure 56 provides a stress contour of the base of the structure at maximum deflection. The maximum stress in the structure does exceed the material yield stress (Figure 56).

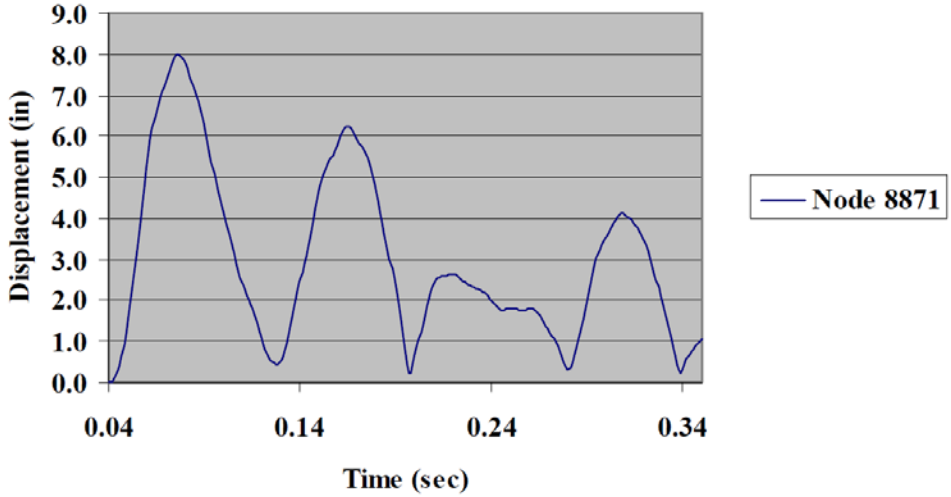

Figure 54. Purlin Translation for 116.8 psi-ms

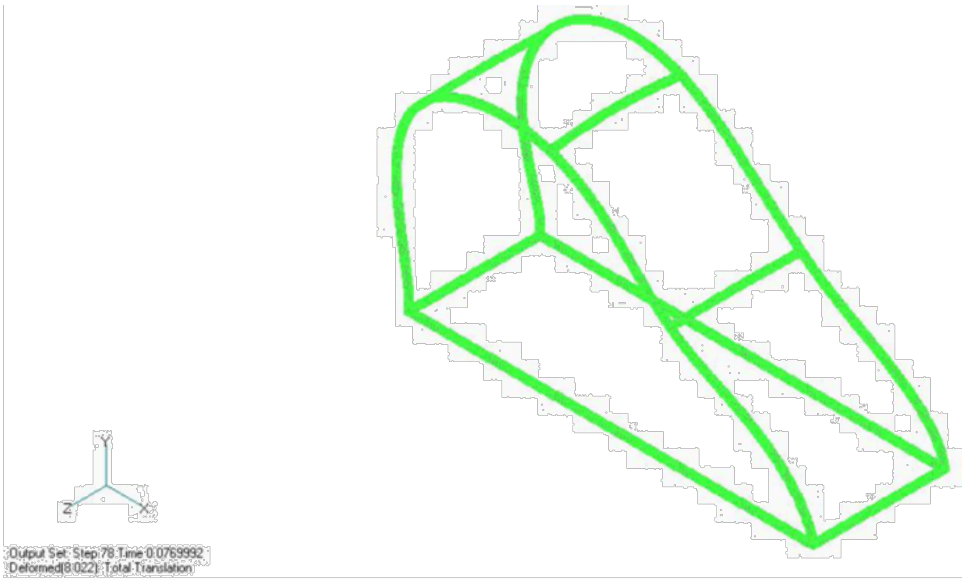

Figure 55. Arch Deflected Shape for 116.8 psi-ms

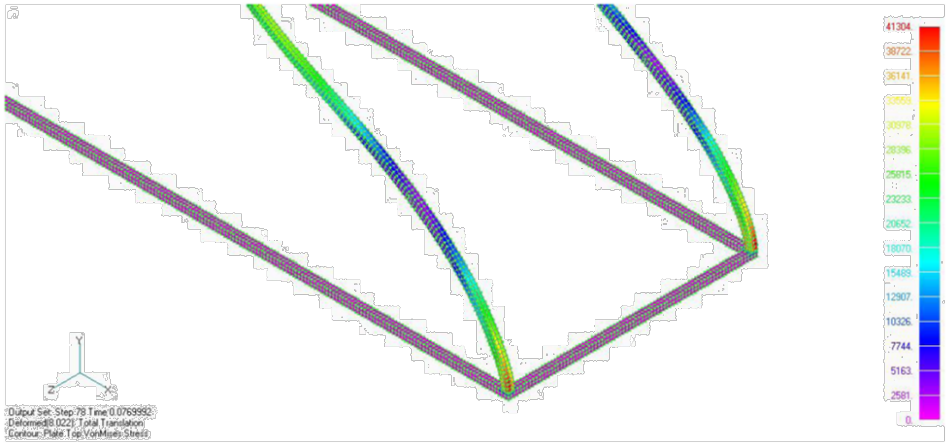

Figure 56. Arch Stress Distribution for 116.8 psi-ms

5.11. 33.1 psi-ms Results

Results for this load case are shown in Figure 57 and Figure 58. This load was chosen to represent an impulse load that should fall into the minor damage region when using the test report prediction curve. Maximum deflection in the structure was approximately 4.0 in, which falls in the minor damage category and is in line with the damage predicted by the test report curve (Figure 57). Figure 58 provides an image of the deformed shape of the structure at approximately 2.4 in of purlin deflection, while Figure 59 provides a stress contour of the structure at approximately 2.4 in of deflection, which corresponds to the maximum deflection for the first peak of the deflection curve. The maximum stress at the base of the structure is less than the material yield stress (Figure 59).

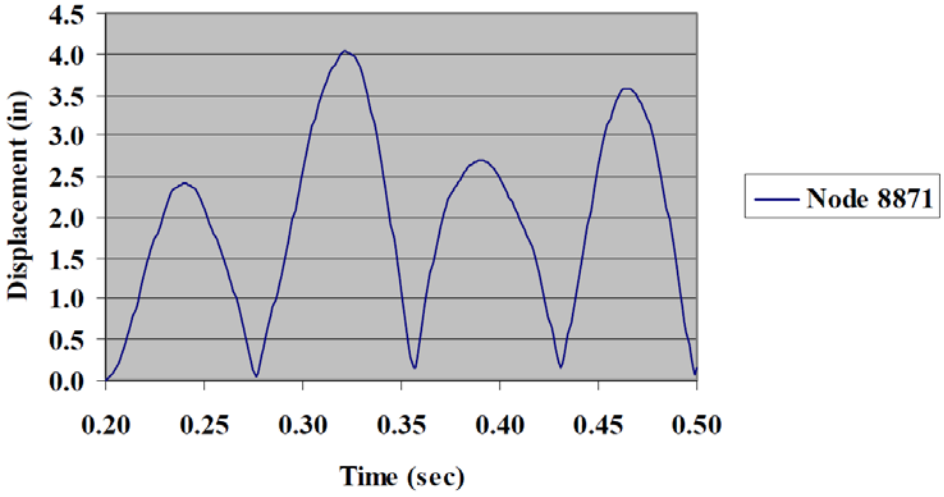

Figure 57. Purlin Translation for 33.1 psi-ms

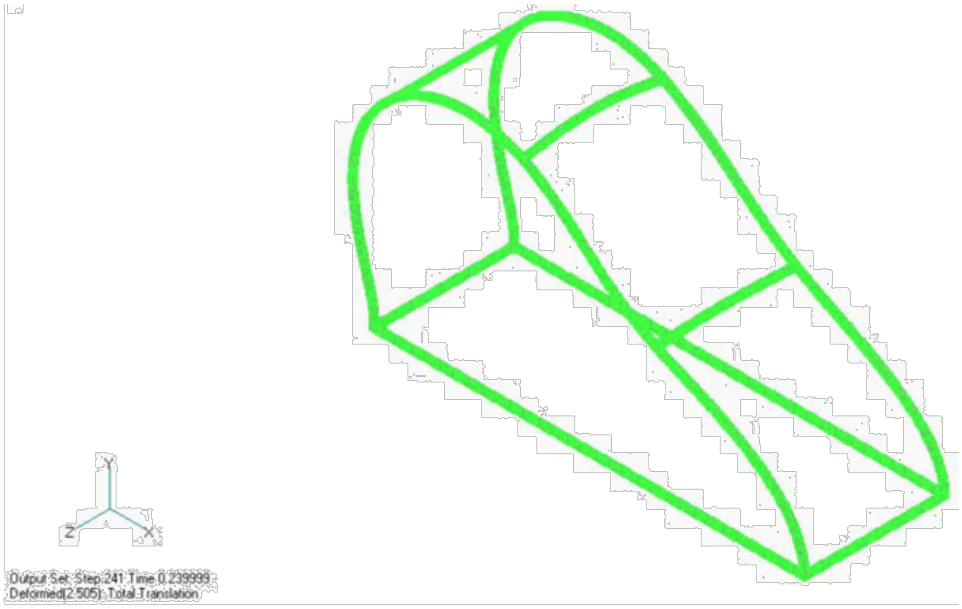

Figure 58. Arch Deflected Shape for 33.1 psi-ms

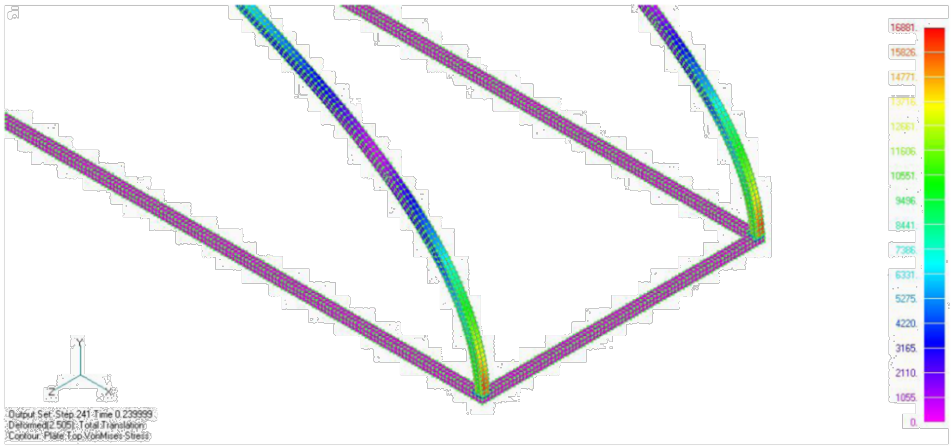

Figure 59. Arch Stress Distribution for 33.1 psi-ms

6. SDOF MODEL VERIFICATION

The goal of this analysis was to develop a simplified model that may be used to predict deflection of the structure under various impulse loadings. A single-degree-of freedom dynamic model will be used in this effort. Section 6.1 provides an analytical development of the SDOF model.

6.1. SDOF Analytical Development

Equation 2 provides the basic equation of motion for a single-degree-of-freedom system with the included terms defined.

$$M_e\ \ddot{y}(t) + C_e\ \dot{y}(t) + K_e\ y(t) = F_e\ (t\ ) \tag{2}$$

M_e = equivalent mass of the SDOF model
$\ddot{y}$(t) = acceleration of the system
C_e = equivalent damping of the system
$\dot{y}$ (t) = velocity of the system
K_e = equivalent stiffness of the system
$y(t)$ = displacement of the system
$F_e(t)$ = equivalent load applied to the system as a function of time

The analysis approach is designed to provide a maximum predicted static deflection at the purlin interface of the structure. Damping in this model does play a role in the initial deflection and will be considered zero for this analysis. Therefore, Equation 2 reduces to Equation 3.

$$M_e\ \ddot{y}(t) + K_e\ y(t) = F_e(t) \tag{3}$$

The equivalent mass, M_e, of the SDOF system representing a system with continuous mass distribution, m, is given by Biggs in Equation 4.

$$M_e = \int^1 m\, \emptyset^2(x)dx \tag{4}$$

The mass factor K_m is defined as the ratio of the equivalent mass to the actual total mass of the structure.

$$\boldsymbol{K_m} = \frac{\boldsymbol{M_e}}{\boldsymbol{M_t}} \tag{5}$$

In the case of a beam with a constant mass along its length, $M_t = mL$, and M_e is given by Equation 4; therefore, the mass factor is given by equation 6.

$$K_m = m \int^L m\, \emptyset^2(x) \frac{dx}{m(L)} = \frac{1}{L} \int^L m\, \emptyset^2(x)dx \tag{6}$$

The equivalent force is given by Equation 7

$$F_e = \int^L w\,(x)\emptyset(x)dx \tag{7}$$

The load factor, K_L, is then defined as the ratio of the equivalent force to the actual force of $F_t=w(x)L$, which for a uniform load becomes $F_t=wL$.

$$K_L = \frac{F_e}{F_t} = \int^L w\,(x)\emptyset(x)\ \ \frac{dx}{w(L)} = \frac{1}{L}\int^L \quad \emptyset(x)dx \tag{8}$$

Biggs defines the resistance of an element, *R*, as the internal force restoring the element to its unloaded static position, and defines it in terms of the load distribution for which the analysis is being made (Biggs, 1964). The stiffness of the element is therefore simply the ratio of the rate of resistance to the incremental change in deflection, Equation 9

$$K = \frac{\Delta R}{\Delta y}\ and\ K_e = \frac{\Delta R_e}{\Delta y} \tag{9}$$

For the beam to be in equilibrium, resistance must always be equal to the force.

$$\frac{F_e}{F_t} = \frac{R_e}{R_t}$$

$$K_L = \frac{K_e}{K_y}(y) \tag{10}$$

Biggs introduces one final factor, which is K_{LM} , the load-mass factor, in order to simplify the equation of motion in terms of that factor alone. K_{LM} is defined as the ratio of the mass factor to the load factor. Equation 3 may now be written in terms of the real system with transformation factors, Equations 5, 8, and 10.

$$K_m M_t \ddot{y}(t) + K_L K y(t) = K_L F(t)$$

Dividing this equation by K_L we arrive at:

$$\frac{\mathrm{K_m M_t \ddot{y}(t)}}{\mathrm{K_L}} + K\,y(t) = F(t) \qquad \mathrm{M_t} = \text{Total mass of system} = m\,L$$

By calling K_{LM} (load-mass factor) = $\frac{K_m}{K_L}$, we arrive at our final equation of motion, Equation 11.

$$K_{LM}\,\mathrm{M_t}\,\ddot{y}(t) + K\,y(t) = F(t) \tag{11}$$

The natural period, *T*, of the system is given by (Biggs, 1964).

$$T = 2\pi\left[\frac{K_{LM}\,M_t}{K}\right]^{\frac{1}{2}}$$

Since the resistance of the system $R\,y = K\,y$, the equation of motion in terms of the resistance of the system is shown is Equation 12.

$$\mathrm{K_{LM}\,M_t\,\ddot{y}(t) + R[y(t)] = F_t} \quad \text{or} \quad \ddot{y}(t) = \frac{F_t}{K_{LM}\,M_t} - \frac{R[y(t)]}{K_{LM}\,M_t} \tag{12}$$

Where K_{LM} = constant that depends on the shape function of the applicable behavior region.

This equation of motion can now be solved numerically for *y(t)*, which gives the total motion-time history of the mass in the idealized system, and is the same as the transverse purlin deflection-time history. The appropriate transformation factors and element stiffness values are applied during the various stages of analysis. The equation of motion can be solved by direct numerical integration. Several numerical integration schemes are described by Biggs (1964), including the constant velocity procedure, the linear acceleration method, the Newmark β method, and several finite difference methods. The Newmark β method is a very versatile method for solving differential equations incrementally. The central difference method corresponds to a Newmark time scheme with parameter values β=0 and γ = ½. The central difference formula relates the acceleration, ÿt at time t to the displacement *yt-Δt*, *yt*, and *yt+Δt* corresponding to displacement at times *t- Δt*, *t*, and *t + Δt*, respectively, according to Equation 13.

$$\ddot{y} = \frac{[y_{t-\Delta t} - 2y_t + y_{t+\Delta t}]}{\Delta t^2} \tag{13}$$

Substituting Equation 13 into Equation 12 and rearranging to solve for $y_{t+\Delta t}$ in terms of $y_{t-\Delta t}$ and y_t yields.

$$y_{t+\Delta t} = \frac{F_t \Delta t^2}{K_{LM}\, M_t} + \left[\frac{2 - R_y \Delta t^2}{K_{LM} M_t}\right] y_t - y_{t-\Delta t} \tag{14}$$

The central difference method is an explicit time scheme because the unknown $\ddot{y}_n$ is only a function of known values. Equation 14 allows for the displacement at the next time increment $y_{t+\Delta t}$ to be calculated in terms of system constants and the current and previous displacement values $y_{t-\Delta t}$ and y_t. Note that F_t is non-zero only when load is being applied to the structure and that R_y is a function of the displacement.

6.2. SDOF Model Term Definition and Calculation

Equation 14 provides the equation of motion for a SDOF model that is used to represent the system. This equation was programmed into Microsoft Excel. The terms included in the SDOF are defined and calculated below for inclusion into the SDOF model.

6.2.1. Applied Force (*Ft*)

F_t is the forcing function applied to the structure as a function of time. The applied force used in the SDOF is derived from the overpressure and time duration calculated by using a spreadsheet program based on the CONWEP Program. This spreadsheet calculated the reflected pressure and time duration based on charge size in pounds of TNT and the distance the charge is located from the structure. The reflected pressure is then multiplied by the exposed area to derive the applied force. Exposed area was calculated as the area of the structure facing the charge with the area reduced by the same function as used to reduce the applied force in the static resistance function calculation.

Area of one arch = $r^*(\theta)^*(2\text{ in}) = 120\text{ in } (1.57\text{ rad})^*\ (2\text{ in})\ 376.8\text{ in}^2$

The distribution of the above area using Equation 1 yields an effective area of 188.4 in^2. Therefore, the two arches have a total effective area of 376.8 in^2. In addition to this area, the area of the two cross members will be added to the exposed area.

Cross member area (CMS) = (2 members) (80 in)(2 in)
CMA = 320 in^2
Total exposed area = 320 in^2 + 376.8 in^2
Total exposed area = 696.8 in^2

$$F_t = (\text{reflected pressure})(\ 696.8\ in^2) \quad (15)$$

6.2.2. Adjusted Time

The load in the SDOF is applied as a right triangle beginning at the maximum load as calculated in Section 6.2.1 and decreasing to zero in a linear manner. Since the area under this right triangle should be equivalent to the reflected impulse (RI), the time duration of the load application is adjusted to create an equivalent area according to Equation 16.

$$Adjusted\ Time\ = \left(\frac{2*RI}{F_t}\right) \quad (16)$$

6.2.3. Load Mass Factor (K_{LM})

The load mass factor is a constant that depends on the shape function of the applicable behavior region. For this effort, K_{LM} is assumed to be the mass participation factor in the *x* direction from the modal analysis of the structure as described in Section 3. The *x* axis is the primary axis of movement in the impulse loading simulation, which is why this participation factor was chosen. Therefore, K_{LM} = 0.47.

6.2.4. System Mass (Mt)

M_t is simply the total mass of the system. For the subject system, the system weight is 123.5 lbs; therefore, M_t = 123.5 lbs / 386.1 in/sec^2 = 0.32 lb-sec^2/in. This final weight excludes the weight of the base restraints in the model.

7. ANALYSIS CHARTS

The SDOF derivation described in Section 6 is implemented in the 11 analyses described in this report using the parameters shown in Table 14

Table 14. SDOF Parameters

Reflected Impulse (psi-ms)	Reflected Pressure (psi)	Adjusted Time Duration (ms)
81.1	33.7	4.8
55.7	15.9	7.0
30.5	6.0	10.2
94.8	7.7	24.6
76.4	5.6	27.2
55.0	3.6	30.6
32.2	1.8	35.8
111.0	30.0	7.4
24.7	2.8	17.6
116.8	18.0	13.0
33.1	2.7	24.5

The inclusion of these parameters resulted in the SDOF results shown in Table 15, which provides the results from the SDOF model as well as the LS-DYNA model such that the two may be compared. In addition to the tabular comparison, Section 7.1 provides graphical comparisons of the results from the two methods (Figure 60–Figure 92).

Table 15. LS-DYNA/SDOF Results Comparison

Impulse (psi-ms)	LS-DYNA Displacement (in)	SDOF Displacement (in)
81.1	4.3	5.3
55.7	3.5	3.5
30.5	3.5	1.8
94.8	10.1	6.1
76.4	8.5	4.5
55.0	6.0	3.2
32.2	3.4	2.2
111.0	6.8	7.1
24.7	3.1	1.5
116.8	8.0	7.9
33.1	4.0	1.9

7.1. Graphical Comparison of LS-DYNA and SDOF Results

The initial conditions for all reflected impulses had an exposed area of 696.8 in^2; a Δt of 0.0001 sec; a M_t of 0.32 $lb/sec^2/in$; a K_{LMe} and K_{LMp} of 0.47; ; a K elastic of 552 lb/in; a K plastic of 485 (lb/in); a K Plastic of 387 (lb/in); a Y elastic limit of 2.32 in; and a Yp plastic of 4.63 in. The remainder of the initial conditions are shown in Table 21.

Table 16. Initial Conditions

Reflected Impulse (psi-ms)	Reflected Pressure (psi)	F_0 (lb)	Adj. Time (sec)
81.1	33.7	23482	0.0048
55.7	15.9	11079	0.007
30.5	6.0	4181	0.01
94.8	7.7	5365	0.025
76.4	5.6	3903	0.027
55.0	3.6	2508	0.031
32.2	1.8	1524	0.036
111.0	30.0	20904	0.007
24.7	2.8	1951	0.018
116.8	18.0	12542	0.013
33.1	2.7	1881	0.025

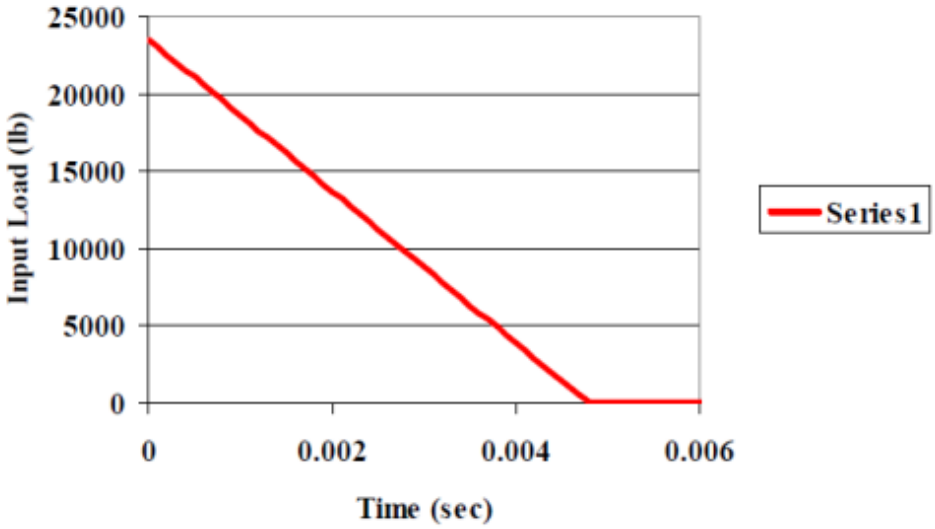

Figure 60. Load Distribution—81.1 psi-ms

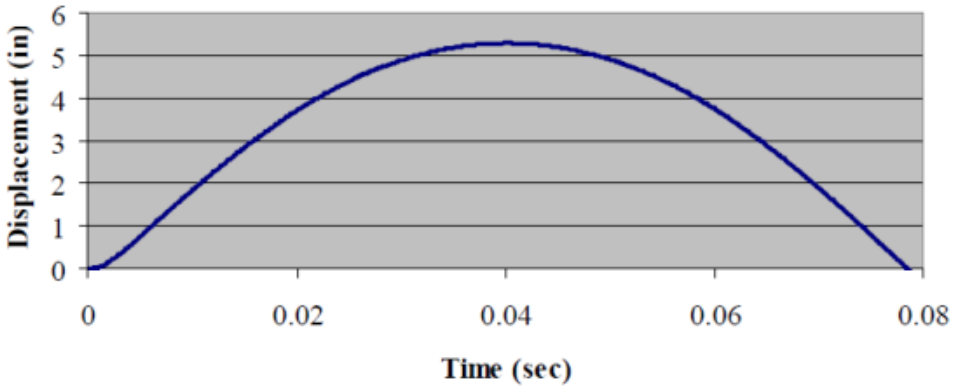

Figure 61. Displacement with Reflected Impulse of 81.1 psi-ms

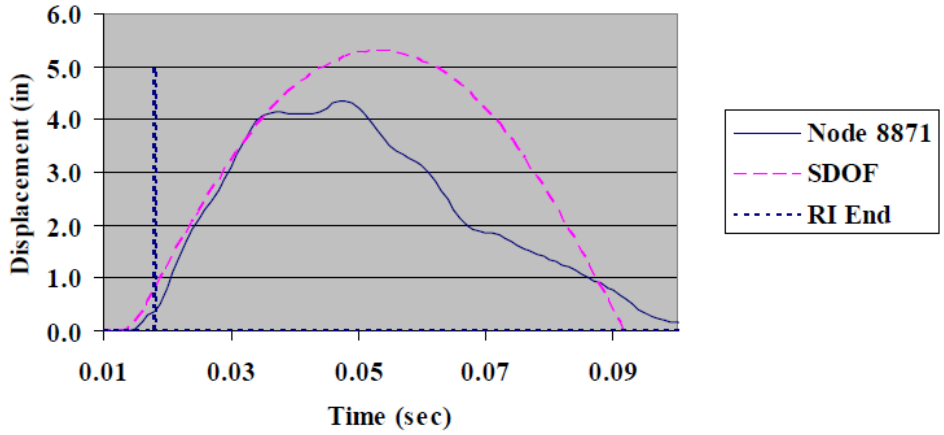

Figure 62. SDOF/LS/DYNA Model Displacement Comparison—81.1 psi-ms

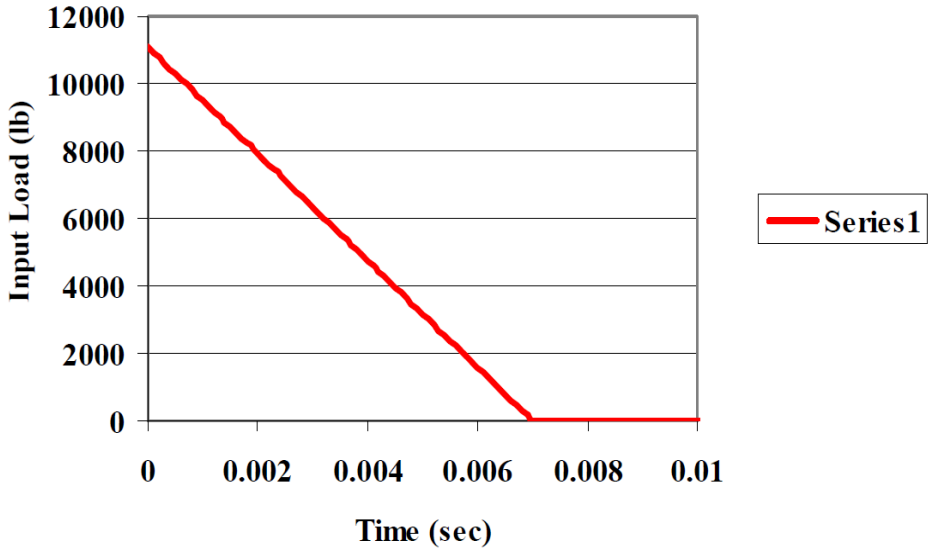

Figure 63. Load Distribution—55.7 psi-ms

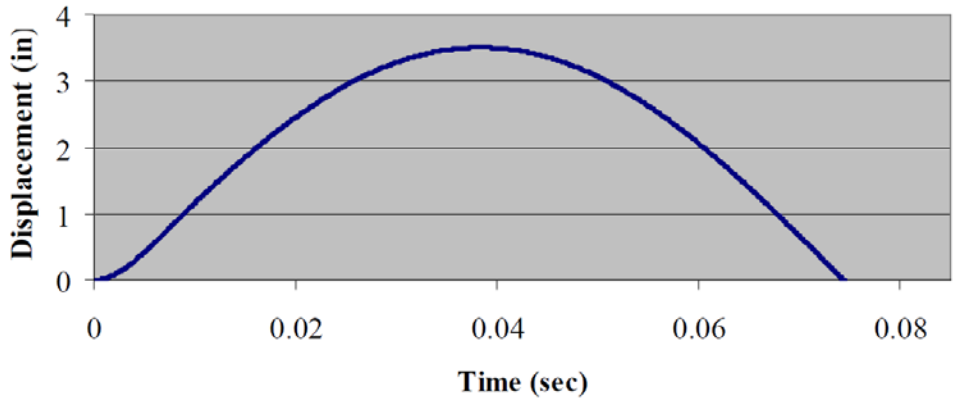

Figure 64. Displacement with Reflected Impulse of 55.7 psi-ms

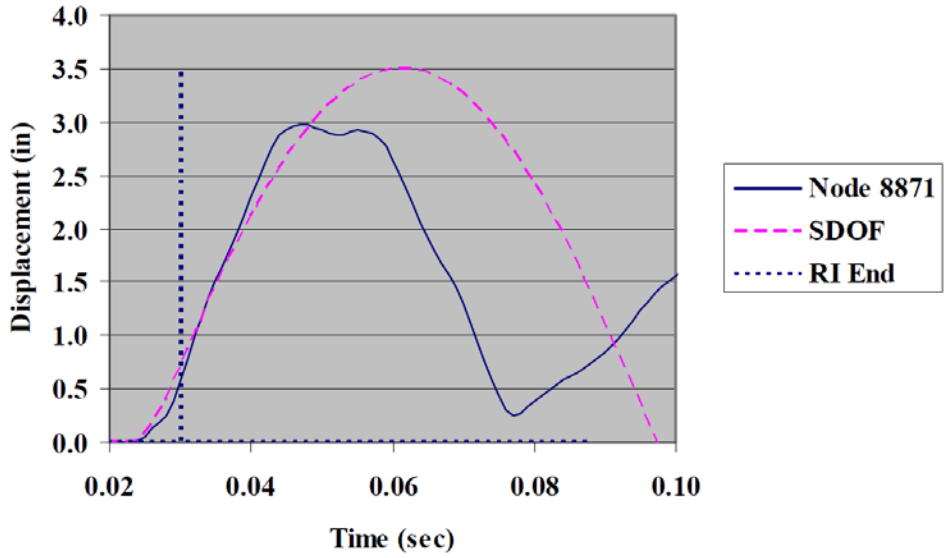

Figure 65. SDOF/LS-DYNA Model Displacement Comparison—55.7 psi-ms

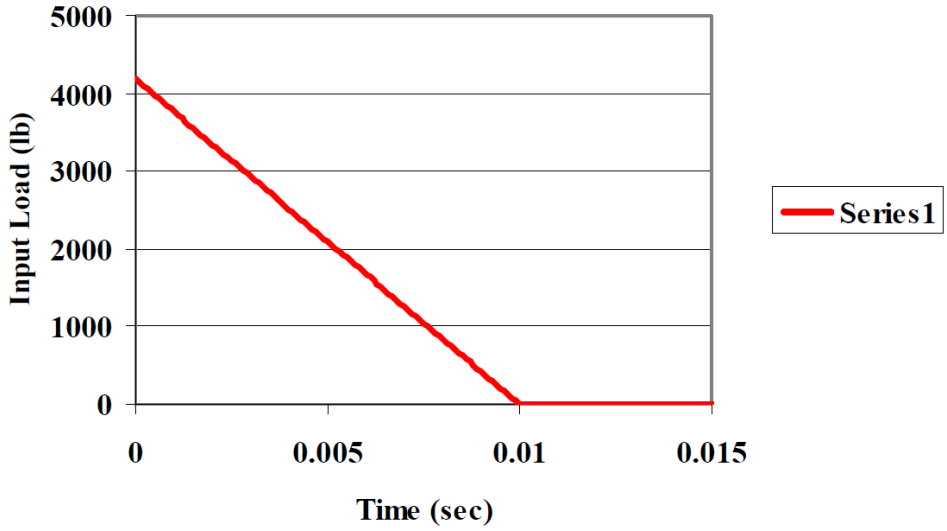

Figure 66. Load Distribution—30.5 psi-ms

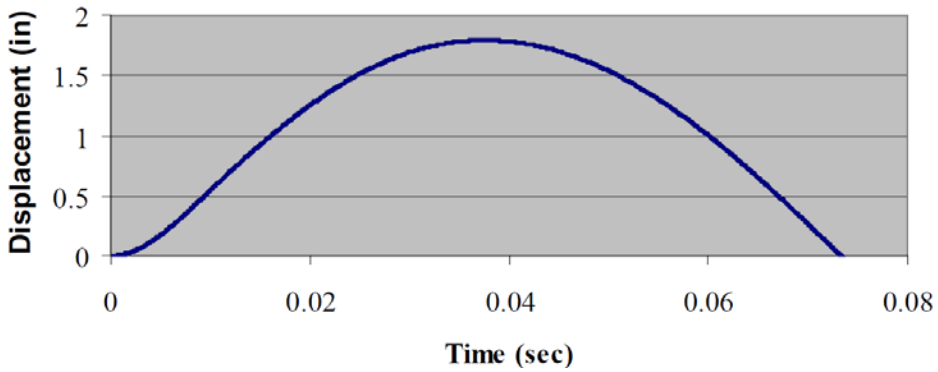

Figure 67. Displacement with Reflected Impulse of 30.5 psi-ms

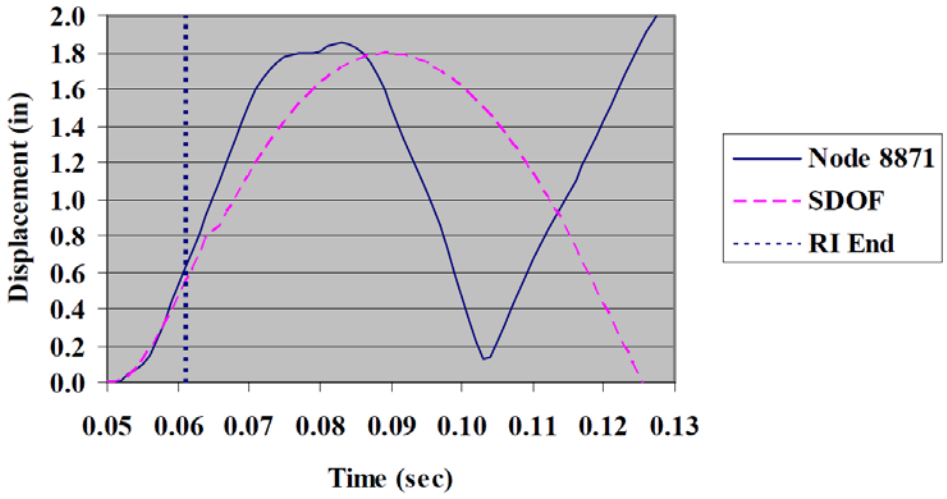

Figure 68. SDOF/LS-DYNA Model Displacement Comparison—30.5 psi-ms

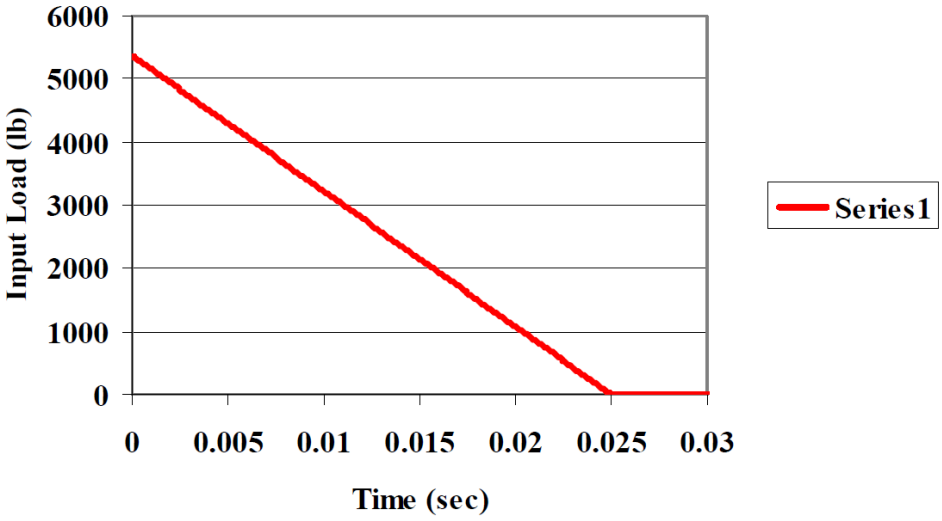

Figure 69. Load Distribution—94.8 psi-ms

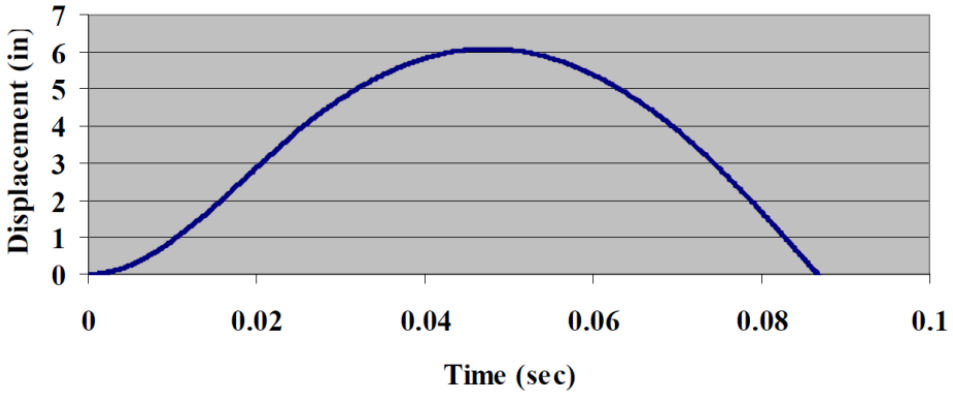

Figure 70. Displacement with Reflected Impulse of 94.8 psi-ms

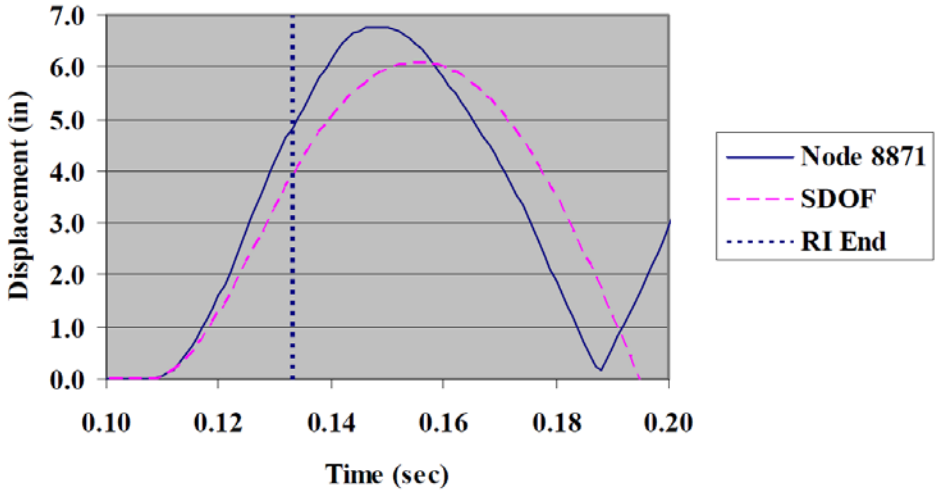

Figure 71. SDOF/LS-DYNA Model Displacement Comparison—94.8 psi-ms

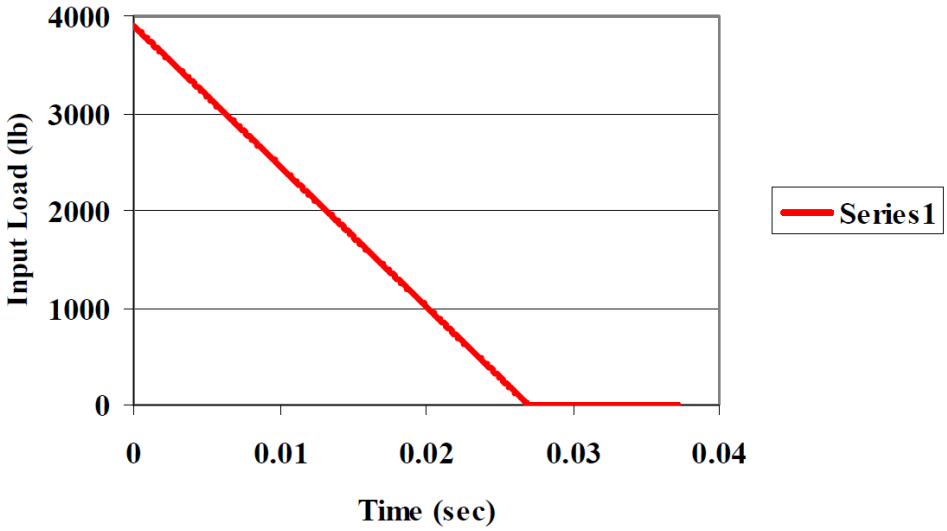

Figure 72. Load Distribution—76.4 psi-ms

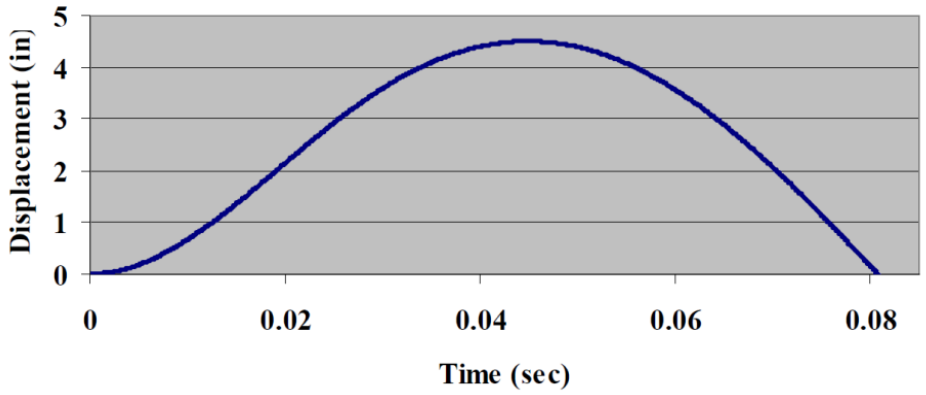

Figure 73. Displacement with Reflected Impulse of 76.4 psi-ms

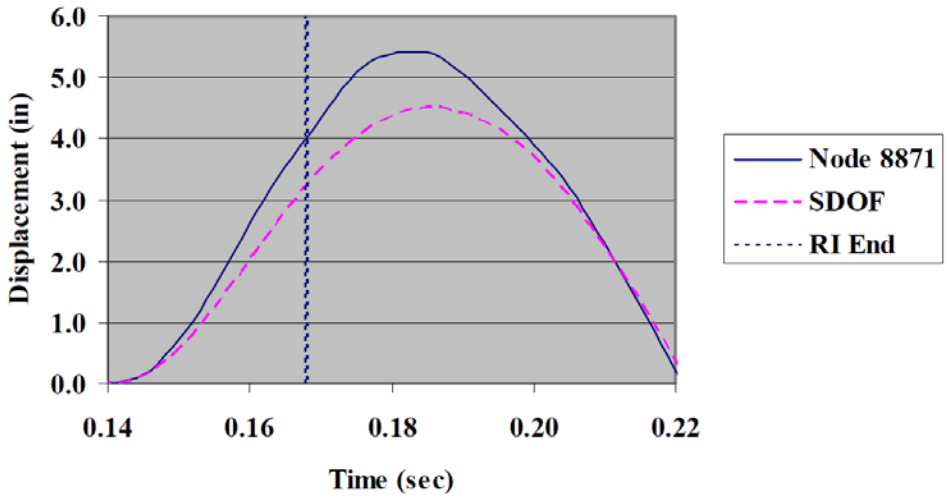

Figure 74. SDOF/LS-DYNA Model Displacement Comparison—76.4 psi-ms

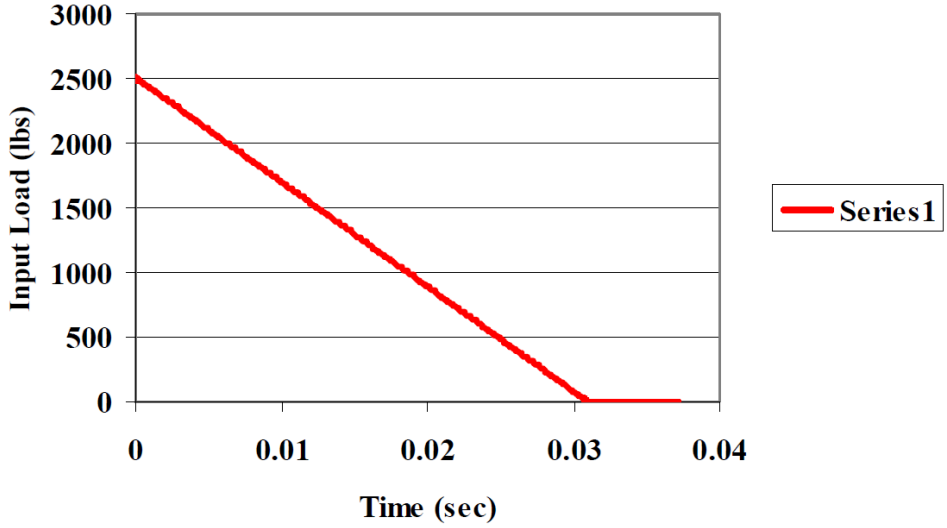

Figure 75. Load Distribution—55.0 psi-ms

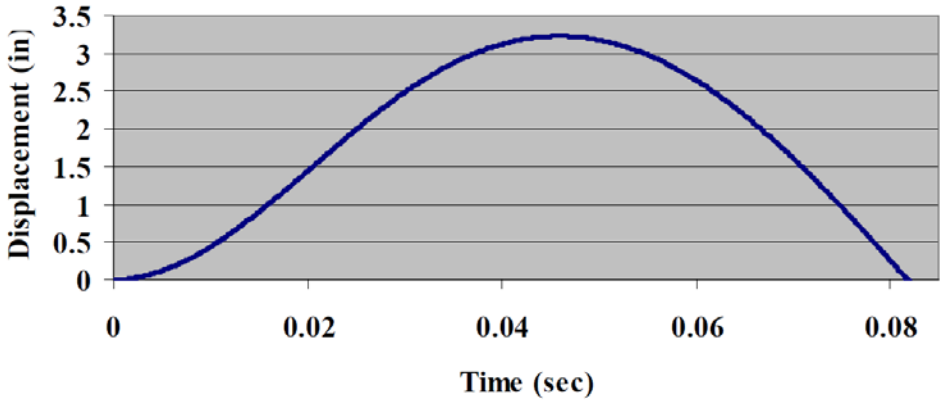

Figure 76. Displacement with Reflected Impulse of 55.0 psi-ms

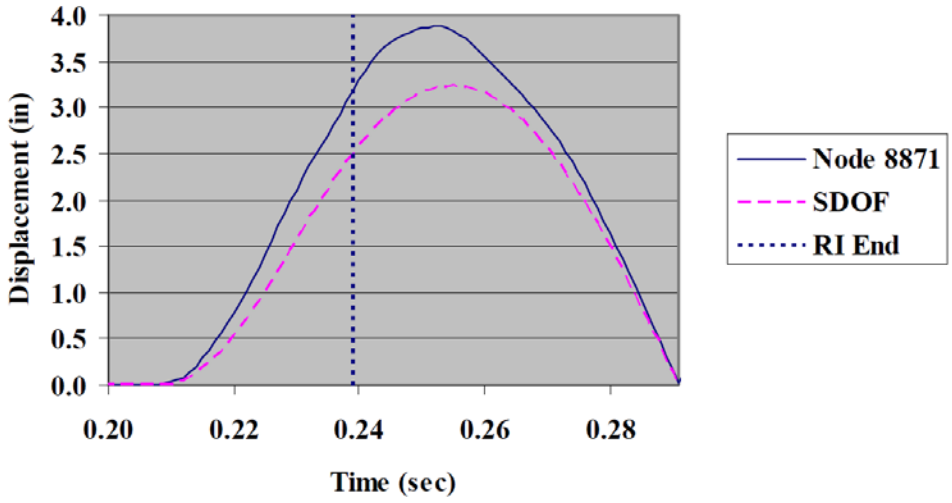

Figure 77. SDOF/LS-DYNA Model Displacement Comparison—55.0 psi-ms

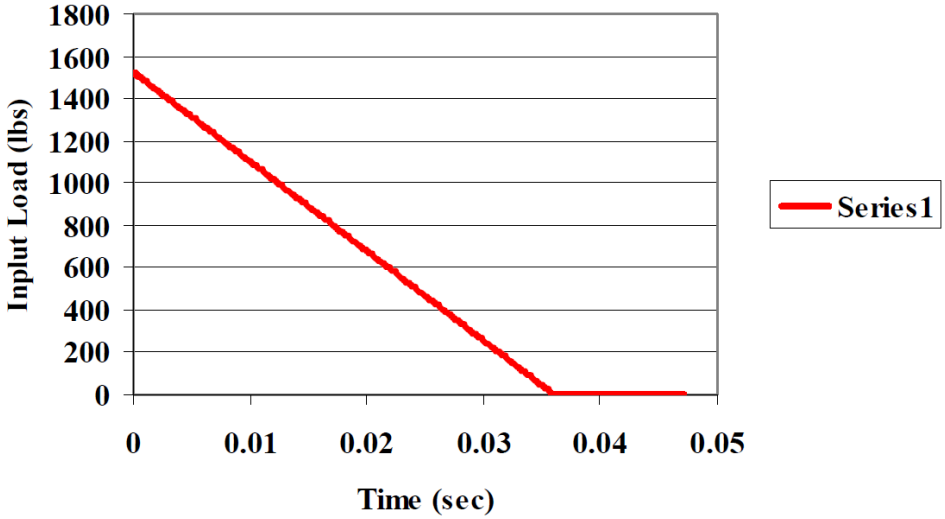

Figure 78. Load Distribution—32.2 psi-ms

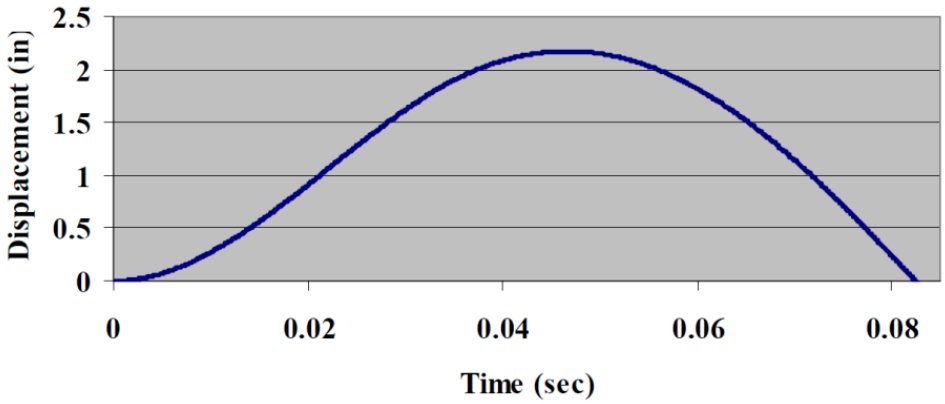

Figure 79. Displacement with Reflected Impulse of 32.2 psi-ms

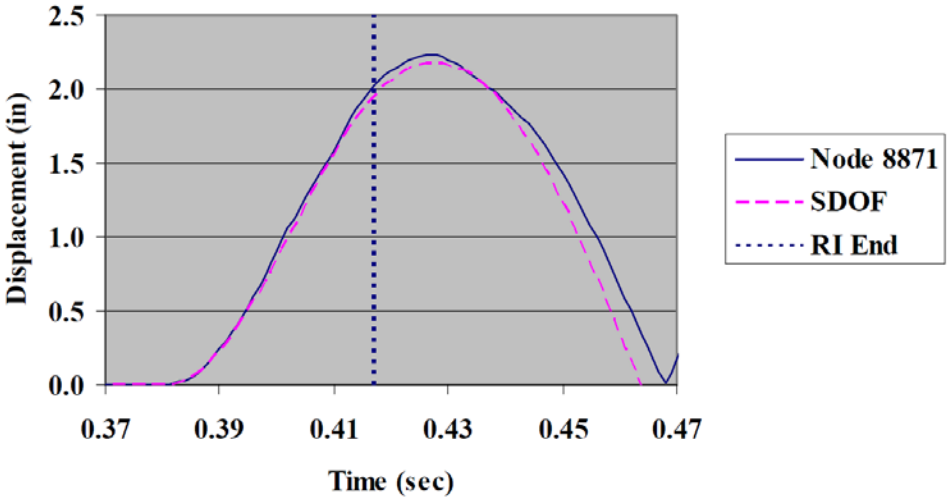

Figure 80. SDOF/LS-DYNA Model Displacement Comparison—32.2 psi-ms

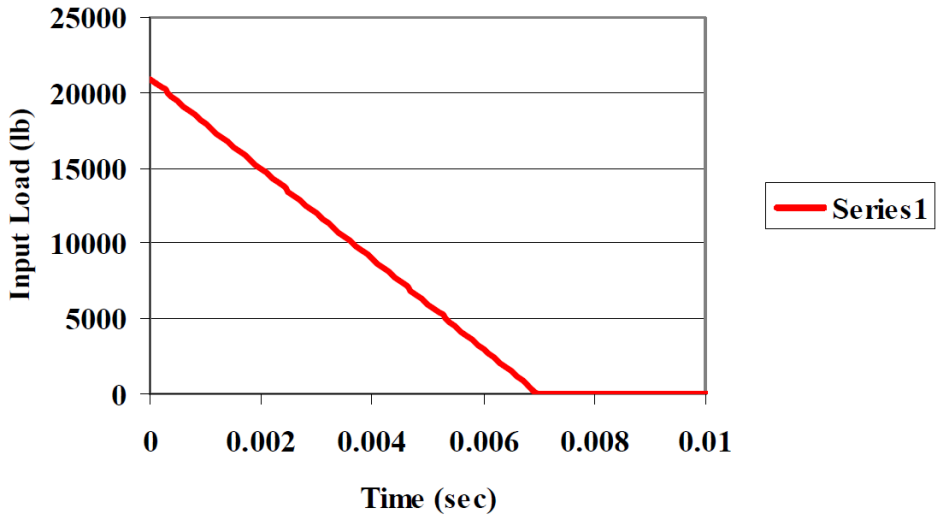

Figure 81. Load Distribution—111.0 psi-ms

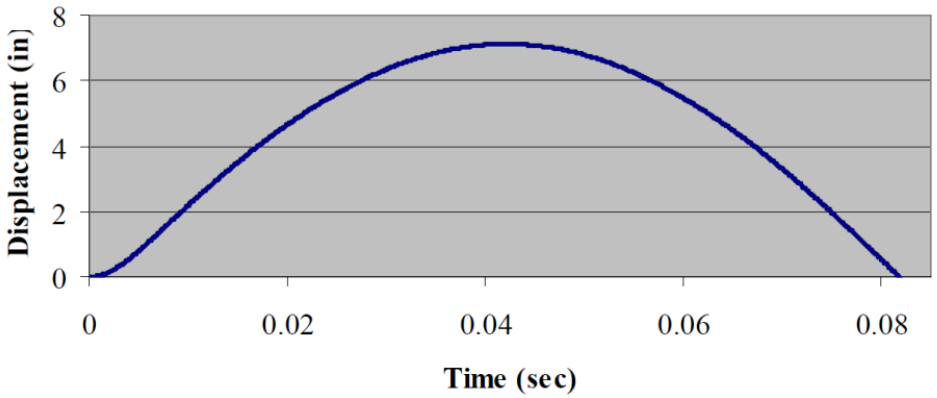

Figure 82. Displacement with Reflected Impulse of 111.0 psi-ms

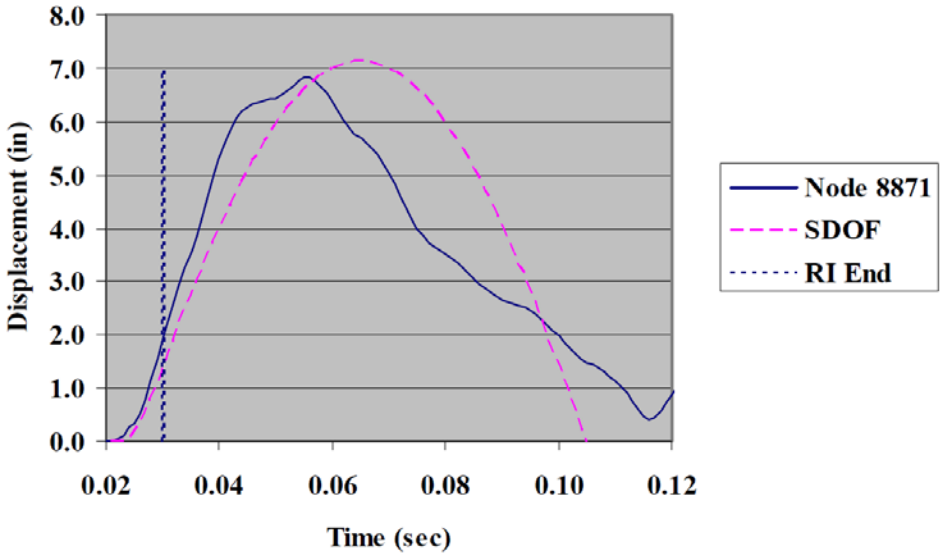

Figure 83. SDOF/LS-DYNA Model Displacement Comparison—111.0 psi-ms

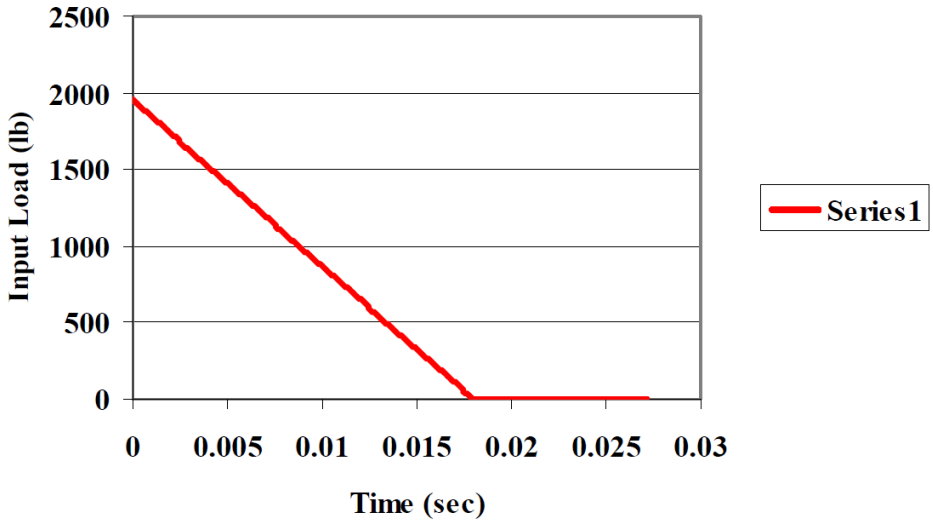

Figure 84. Load Distribution—24.7 psi-ms

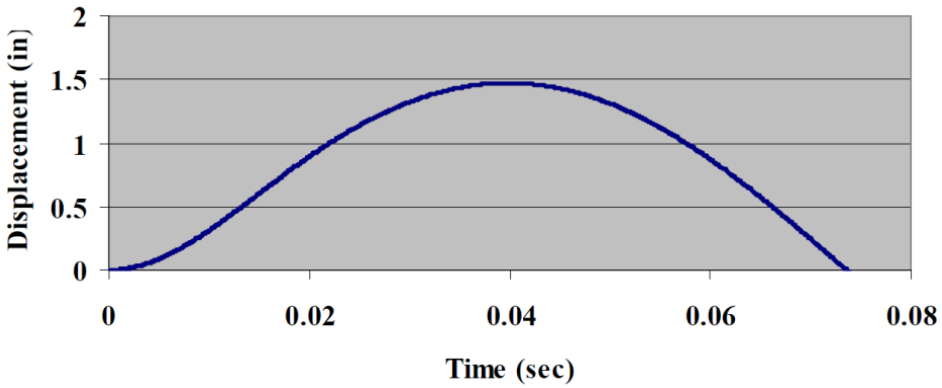

Figure 85. Displacement with Reflected Impulse of 24.7 psi-ms

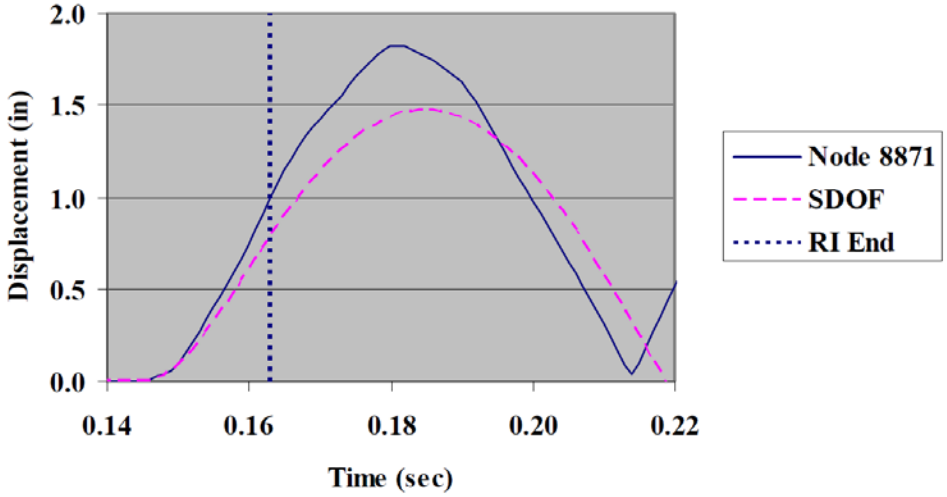

Figure 86. SDOF/LS-DYNA Model Displacement Comparison—24.7 psi-ms

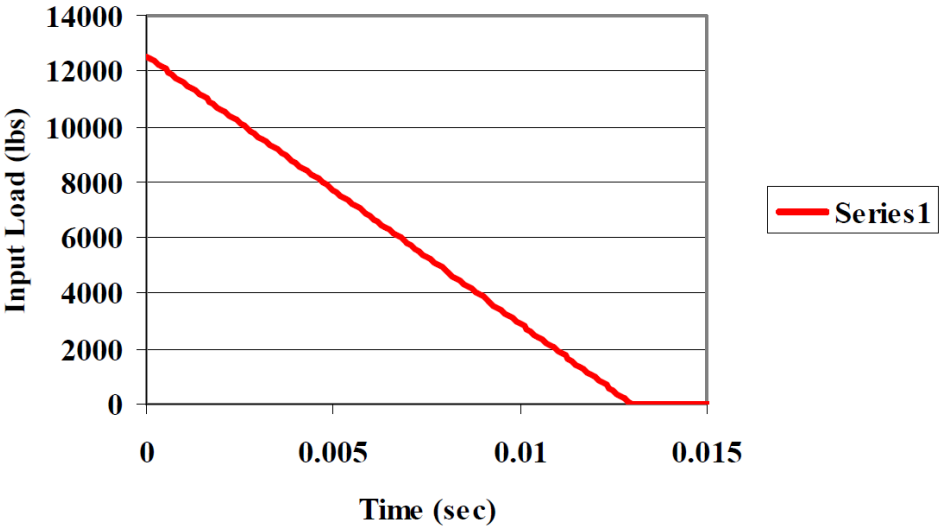

Figure 87. Load Distribution—116.8 psi-ms

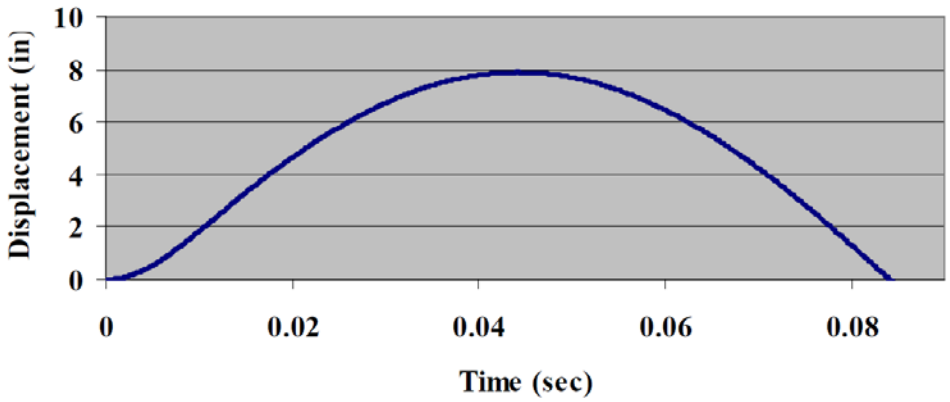

Figure 88. Displacement with Reflected Impulse of 116.8 psi-ms

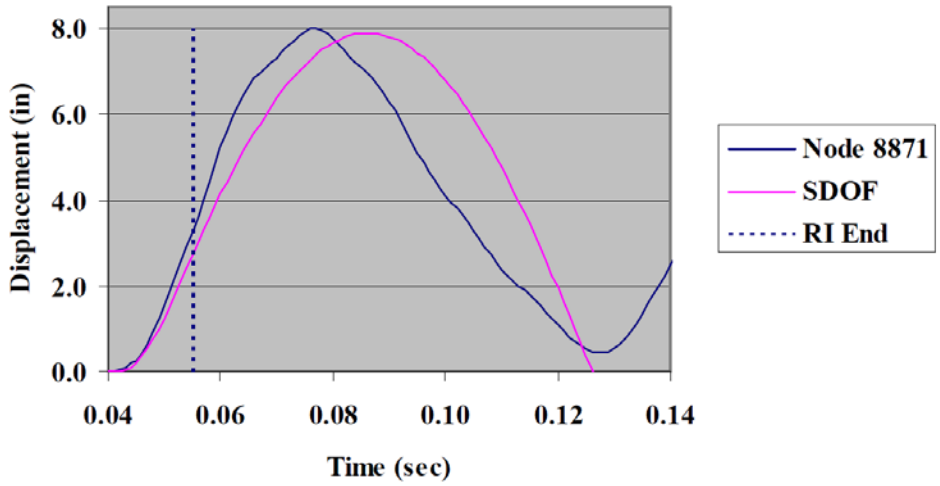

Figure 89. SDOF/LS-DYNA Model Displacement Comparison—116.8 psi-ms

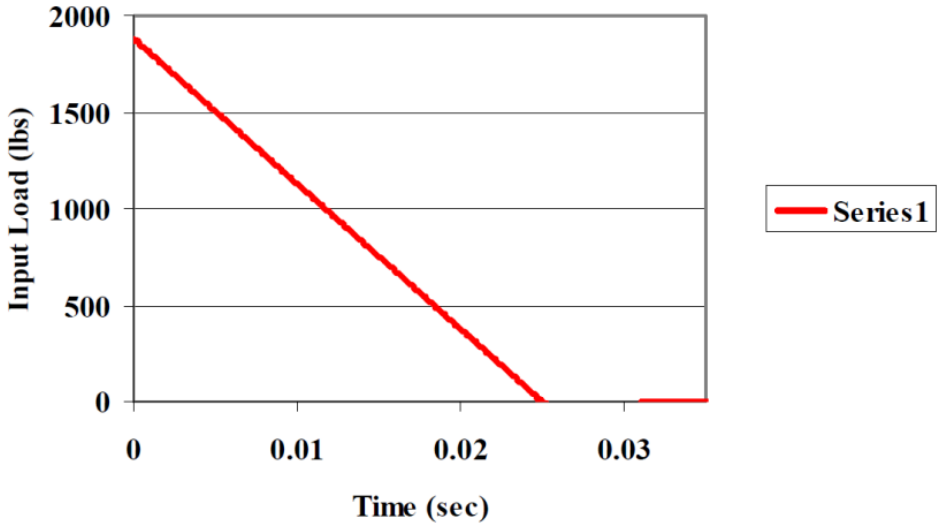

Figure 90. Load Distribution—33.1 psi-ms

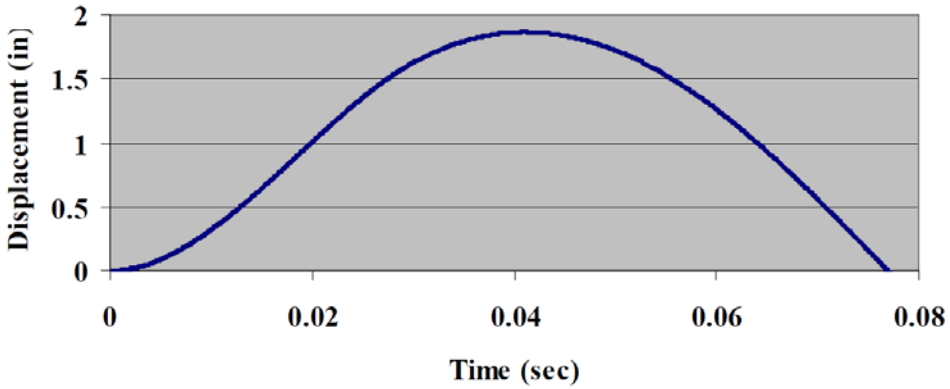

Figure 91. Displacement with Reflected Impulse of 33.1 psi-ms

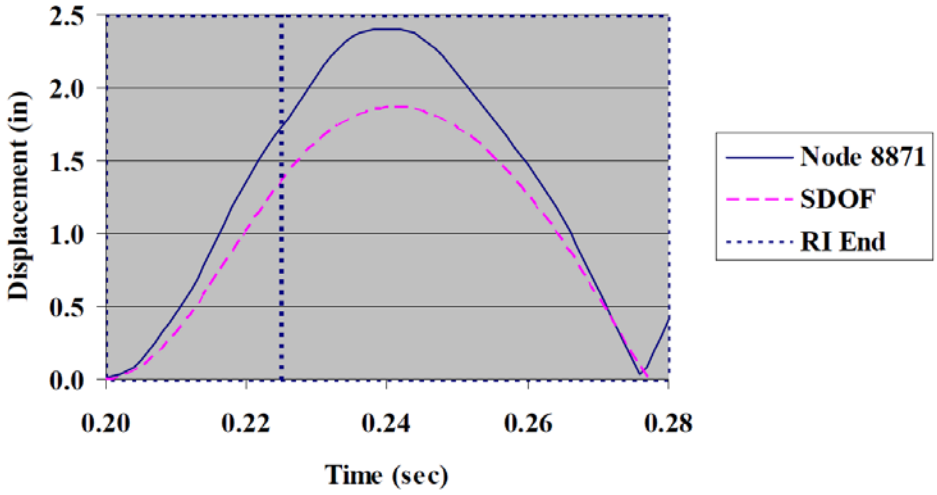

Figure 92. SDOF/LS-DYNA Model Displacement Comparison—33.1 psi-ms

8. SUMMARY AND CONCLUSIONS

The results of this effort to correlate the data generated by field testing of multiple charge sizes and stand-off distances to analytical results obtained from finite element modeling and SDOF models supports the conclusion that simple analytical tools may be developed to predict the behavior of structures. The comparison between FEM and SDOF consistently showed good correlation for the first oscillation of the frame. However, due to the differences in the overall magnitude of the deflection, more effort should be placed in the development of the resistance function. This should include a more refined load distribution as opposed to the simple parabolic distribution described in this report.

9. REFERENCES

1. Blast Response of Air Force Expeditionary Structures to Explosive Loading, Joint Soldier Protection in Contingency Environments, AFRL-ML-TY-TR-2005- 4572, August 2005.
2. Biggs (1964), Introduction to Structural Dynamics, McGraw-Hill Book Company, New York
3. Metallic Materials and Elements for Flight Vehicle Structures, MIL-HDBK-5H, December 1998.

LIST OF SYMBOLS, ABBREVIATIONS, AND ACRONYMS

AFRL	Air Force Research Laboratory
AKSSS	Alaska Small Shelter System
CONWEP	conventional weapons effect
ERDC	Engineer Research and Development Center
FEM	finite element model
FEMAP	finite element modeling and post processing software
NASTRAN	NASA Structural Analysis Program
SDOF	single degree of freedom
SPICE	Soldier Protection in Contingency Environments
TNT	trinitrotoluene
USAF	United States Air Force